NAVAL POSTGRADUATE SCHOOL

MONTEREY, CALIFORNIA

THESIS

THE REFRACTIVE EFFECTS OF LASER PROPAGATION THROUGH THE OCEAN AND WITHIN THE OCEAN

by

Pavlos Xiradakis

December 2009

Thesis Advisor:	Donald Walters
Second Reader:	Brett Borden

Approved for public release; distribution is unlimited

REPORT DOCUMENTATION PAGE			Form Approved OMB No. 0704-0188
Public reporting burden for this collection of information is estimated to average 1 hour per response, including the time for reviewing instruction, searching existing data sources, gathering and maintaining the data needed, and completing and reviewing the collection of information. Send comments regarding this burden estimate or any other aspect of this collection of information, including suggestions for reducing this burden, to Washington headquarters Services, Directorate for Information Operations and Reports, 1215 Jefferson Davis Highway, Suite 1204, Arlington, VA 22202-4302, and to the Office of Management and Budget, Paperwork Reduction Project (0704-0188) Washington DC 20503.			
1. AGENCY USE ONLY ***(Leave blank)***	**2. REPORT DATE** December 2009	**3. REPORT TYPE AND DATES COVERED** Master's Thesis	
4. TITLE AND SUBTITLE The Refractive Effects of Laser Propagation through the Ocean Surface and within the Ocean		**5. FUNDING NUMBERS**	
6. AUTHOR(S) Pavlos Xiradakis			
7. PERFORMING ORGANIZATION NAME(S) AND ADDRESS(ES) Naval Postgraduate School Monterey, CA 93943-5000		**8. PERFORMING ORGANIZATION REPORT NUMBER**	
9. SPONSORING /MONITORING AGENCY NAME(S) AND ADDRESS(ES) N/A		**10. SPONSORING/MONITORING AGENCY REPORT NUMBER**	
11. SUPPLEMENTARY NOTES The views expressed in this thesis are those of the author and do not reflect the official policy or position of the Department of Defense or the U.S. Government.			
12a. DISTRIBUTION / AVAILABILITY STATEMENT Approved for public release; distribution is unlimited		**12b. DISTRIBUTION CODE**	

13. ABSTRACT (maximum 200 words)

This thesis investigates the effect of the ocean water attenuation on a laser beam fired upward inside the ocean. The laser beam spreading due to scattering is approximated. The method used is a computer Monte Carlo simulation. Angular spreading of light caused by refraction at the sea surface is also studied and compared with the ocean results. The method is to simulate geometrical light rays passing through a randomly realized ocean surface wave model and derive statistics of the angular refraction. The results of this work can be used for detection of objects in the water and laser communication to submerged objects from an airborne or space platform.

14. SUBJECT TERMS ocean waves, laser, scattering, absorption, refraction			**15. NUMBER OF PAGES** 73
			16. PRICE CODE
17. SECURITY CLASSIFICATION OF REPORT Unclassified	**18. SECURITY CLASSIFICATION OF THIS PAGE** Unclassified	**19. SECURITY CLASSIFICATION OF ABSTRACT** Unclassified	**20. LIMITATION OF ABSTRACT** UU

NSN 7540-01-280-5500 Standard Form 298 (Rev. 2-89)
Prescribed by ANSI Std. 239-18

THIS PAGE INTENTIONALLY LEFT BLANK

Approved for public release; distribution is unlimited

THE REFRACTIVE EFFECTS OF LASER PROPAGATION THROUGH THE OCEAN AND WITHIN THE OCEAN

Pavlos Xiradakis
Lieutenant Junior Grade, Hellenic Navy
Bachelor of Naval Science, Hellenic Naval Academy, 2001

Submitted in partial fulfillment of the
requirements for the degree of

MASTER OF SCIENCE IN PHYSICS

from the

NAVAL POSTGRADUATE SCHOOL
December 2009

Author: Pavlos Xiradakis

Approved by: Donald Walters
Thesis Advisor

Brett Borden
Second Reader

Andres Larazza
Chairman, Department of Physics

THIS PAGE INTENTIONALLY LEFT BLANK

ABSTRACT

This thesis investigates the effect of the ocean water attenuation on a laser beam fired upward inside the ocean. The laser beam spreading due to scattering is approximated. The method used is a computer Monte Carlo simulation. Angular spreading of light caused by refraction at the sea surface is also studied and compared with the ocean results. The method is to simulate geometrical light rays passing through a randomly realized ocean surface wave model and derive statistics of the angular refraction. The results of this work can be used for detection of objects in the water and laser communication to submerged objects from an airborne or space platform.

THIS PAGE INTENTIONALLY LEFT BLANK

TABLE OF CONTENTS

LIST OF FIGURES

LIST OF TABLES

THIS PAGE INTENTIONALLY LEFT BLANK

ACKNOWLEDGMENTS

I am grateful to Professor Walters for his guidance and patience throughout this difficult but beneficial procedure. Without him, this work would never be completed properly. I would also like to thank Professor Brett Borden and LT Paul Blodgett for their help. Finally, how could I forget my wife, Marianthi, who was standing by me all these twenty-seven months at NPS.

THIS PAGE INTENTIONALLY LEFT BLANK

I. INTRODUCTION

A. OVERVIEW

Laser detection of objects in the water and laser communication to submerged objects from an airborne or space platform requires that the laser beam traverse the air-ocean surface on the way to the object. In addition, the scattered energy of a source below the surface must traverse the ocean on the upward return path. The rough ocean surface spreads the laser energy. Once the laser beam has entered the ocean, the turbid water scatters the energy, further spreading the laser beam. The relative significance of these two processes, and the angular spread of a laser beam, depends on the depth of the object, the ocean turbidity and the size of the beam on the ocean surface.

B. THESIS OBJECTIVE

To investigate the beam spread versus angle of incidence, this thesis proposes to simulate the angular, refractive effects of laser energy passing through the ocean surface and the scattering within the ocean. The dependence of the beam size on the ocean surface and depth of the object below the surface will be considered. The primary approach will be to simulate the ocean surface with different models of the spectrum of the ocean surface waves. Analogous to atmospheric wave-optical laser propagation codes, a representation of the ocean surface can be simulated by starting with Gaussian random numbers low pass filtered by realistic ocean surface wave spectra. Fourier transforming back into x, y coordinates provides a simulated ocean surface. Using ray-optics, the trajectories of a sequence of optical rays will reveal the angular dispersion of the ocean surface waves. Both 1-D and 2-D spectral representations of the ocean waves will be considered. After the refractive effects of the ocean surface waves are considered, the effects of the volume scattering will be included using the known scattering functions for the ocean.

The final goal is to develop a realistic probability distribution for the angular spreading of the laser beam including the turbid scattering as a function of the depth of the object. This is coupled with the ocean surface refractivity and the size of the laser beam footprint on the ocean surface.

C. THESIS OUTLINE

The structure of this thesis is organized into the introduction, background (Chapter II) and four additional chapters. Chapter III examines the wind-generated ocean surface. Starting from an already known spectrum, a surface model suitable for the scope of this thesis will be approximated. In Chapter IV, the air water interaction at the ocean surface will be examined, using Snell's Law. Chapter V contains the analysis of scattering and absorption phenomena inside the water body. A Monte Carlo simulation will be used. Next, refraction at the surface will be again evaluated, this time including scattering and absorption. Finally, in Chapter VII the conclusions, based on the results obtained from the analysis in the previous chapters, are presented.

II. BACKGROUND

In this chapter, some of the background knowledge, terminology and basic concepts of optical oceanography are introduced.

As light reaches the earth's surface, there is a 70% probability of striking a water surface and interacting with water. At this interface, various phenomena may occur: A brief description of them will be presented next.

A. INHERENT AND APPARENT OPTICAL PROPERTIES

Inherent optical properties are those whose values are not affected by the distribution of radiance at any given point. Among them, the most important concerning our work are the absorption coefficient (α), the scattering coefficient (b) and the normalized volume scattering function $\tilde{\beta}(\theta)$. The nature of the light field inside a water mass, given the incident light radiation, is a function of these properties.

The apparent optical properties, in contrast with the inherent ones, are those whose value at any given point in the medium depends on the radiance distribution at that point. These cannot be regarded as properties of the water itself but of the light distribution inside the water. Typically, the vertical attenuation coefficient is examined for the downward irradiance and the irradiance reflectance.

It is possible to calculate the inherent properties from readily observed and measured apparent properties. The way in which the observed properties depend on fluctuations of the inherent properties can also be estimated.

A detailed description and mathematical expression of all the above properties and the fundamental quantities, whose knowledge is essential for this work, is presented in Appendix A.

B. REFRACTION AT THE SEA SURFACE

The interface between the sea water and the air includes two media with different optical densities. Due to the different velocity of propagation in these two media, light

that penetrates in a water body changes its direction. This is according to Snell's Law: $n_\alpha \sin\phi_a = n_\alpha \sin\phi_a$, as shown in Figure 1.

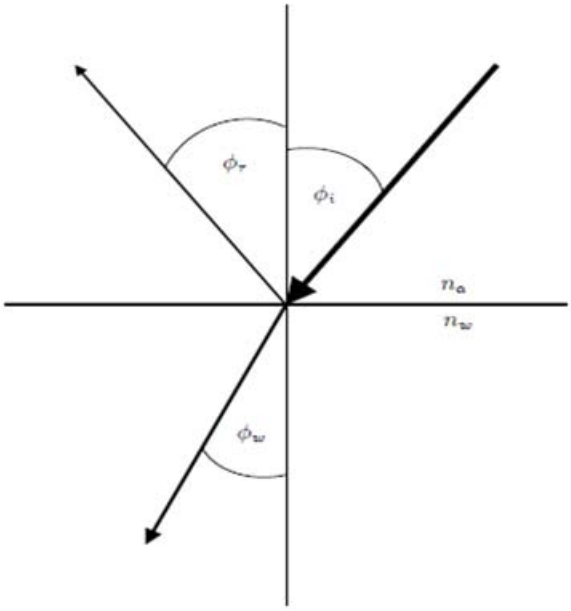

Figure 1. Snell's Law and the reflection law

where φ_α and φ_ω correspond to the angle of incidence and refraction, respectively.

n_α and n_ω are the refractive indices of air and water respectively. These indices vary with temperature, salinity and wavelength. For all practical purposes, the above effects can be neglected by assuming that water has a constant refractive index of 1.33. The above law holds for both directions (light entering or exiting the water surface).

C. REFLECTION AT THE SEA SURFACE

According to the reflection law, the light beam is reflected at the same angle with the angle of incidence, as shown in Figure 1. The reflected electric vector generally has one component parallel and one perpendicular to the plane of incidence, given by Fresnel's equations.

Reflection at the sea surface depends on the solar elevation, the existence of waves on the sea surface and on the wavelength (dispersion). Furthermore, in bad weather conditions, it is difficult to discriminate the true reflectance from the short wave back-scattered light from the sea surface. Figure 2 exhibits the solar elevation dependence of the reflection. The parameter n is the significant ratio of sky radiation to global radiation.

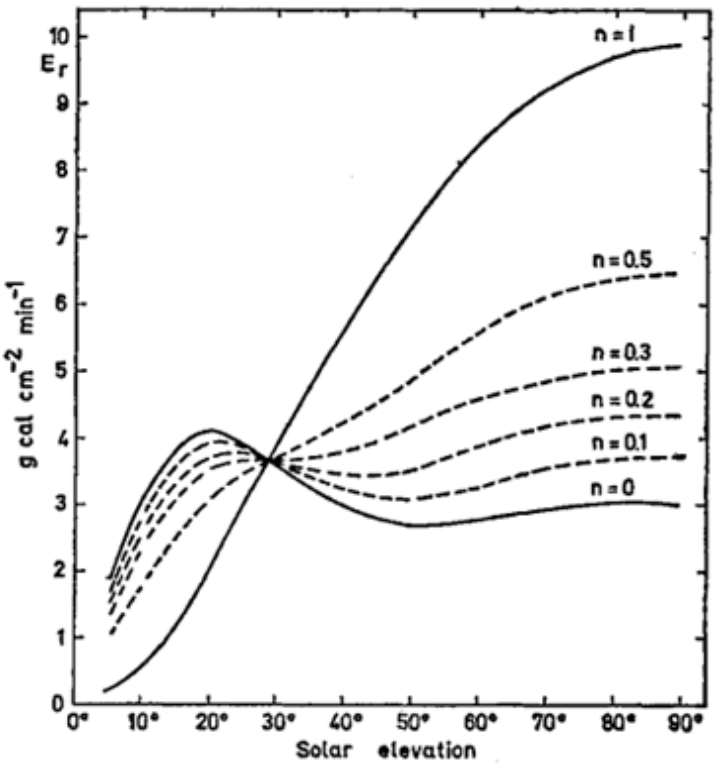

Figure 2. Amount of reflected Energy as a function of the solar elevation for various values of the ratio n of sky radiance to global radiation. (From [1])

1. Sun Glitter

Glitter is a special reflection phenomenon. It takes place when a flat water surface is roughened by the wind. The sun image, formed by specular reflection, has many distinct glittering points. As the water surface becomes rougher, the phenomenon is more obvious and the glittering band increases. The phenomenon was used by Cox and Munk for estimating the sea surface slope.

2. Dispersion of Reflection

For angles lower than 30 degrees, observations show that irradiance reflection depends on the wavelength. This dispersion is common to other phenomenon concerning the light and water interaction, such as scattering and attenuation.

D. SCATTERING

Scattering and absorption are the two main processes that determine light propagation inside the ocean. Scattering involves the abrupt deviation of light from rectilinear propagation. It changes the direction of photon transport, “dispersing” them as they penetrate a sample, without changing their wavelength. The scattering coefficient, b(λ), is equal to the fraction of energy dispersed from a light beam per unit of distance traveled in a scattering medium, in m^{-1}.

The most important parameter concerning scattering is the volume scattering function, which represents scattering as a function of the scattering angle. Important quantities concerning scattering are presented in Appendix A.

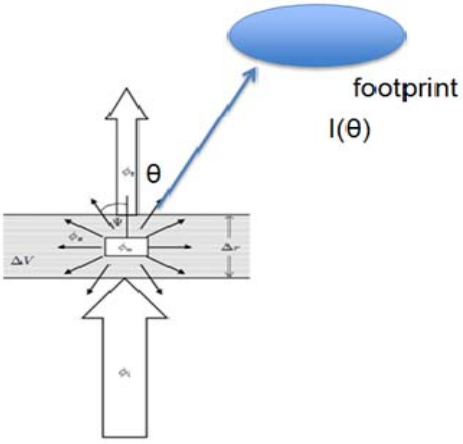

Figure 3. A beam of light with Intensity Φ_i enters a medium of volume ΔV. Part of the light is absorbed inside the medium (Φα), part of the light is scattered at various angles Ψ and a part is transmitted outside the medium (Φt).The exiting rays create an elliptical footprint. (After [2])

1. Geometric Optics' Scattering

The scattering process is the result of the following procedures: Diffraction, where light is reradiated from rectilinear propagation; Refraction, where light penetrates the object and emerges with or without internal reflections; Finally, reflection, where light does not penetrate.

2. Scattering in Sea Water

Scattering in sea water is produced by the water itself and the suspended particles as well. Since small particles produce wide angle scattering, the scattering by particles is far more important. Particle scattering is mainly dependent on the particle concentration, particle size and optical radiation wave length. The major effect comes from particles with size greater than the wavelength of light. Absorption should be taken into

consideration as well. Diffraction is largely independent of the composition of the particle, where refraction and reflection are determined by the refractive index of the particle.

3. Scattering by Water Background

a. Rayleigh Theory

Rayleigh scattering can be considered as a molecular problem. According to Rayleigh theory, a homogenous electrical field E induces in each particle an oscillating dipole, which radiates in all directions. In the case of N particles with a smaller size compared to the wavelength of the incident radiant energy, the radiant intensity in the θ direction (angle respectively to the horizontal) is given by [3]

$$I = \frac{8\pi^4 \mathrm{N}\alpha^2 \mathrm{E}^2}{\lambda^4}(1+\cos^2\theta) \quad \text{W/St} \tag{3.1}$$

where α is the polarizability of the particle.

b. Fluctuation Theory

This theory relates scattering with fluctuations in density of concentration in a small volume element of the fluid. Regarding intensity distribution and polarization, scattering has the same properties with Rayleigh theory. The volume scattering function is given from [3]

$$\beta_0(\theta) = \frac{\pi^2 \nu k T}{18\lambda^4}(n^2-1)^2(n^2+2)^2(1+\cos\theta)$$

where ν is the thermal compressivity, k is the Boltzmann constant, n is the refractive index and T is the absolute temperature. This theory declares that scattering also depends on Temperature and pressure and is more suitable for liquids scattering.

c. Mie Theory

The total scattered radiation in the θ direction from a randomly polarized beam will be [3].

$$I = \frac{\lambda^2}{4\pi}\int_0^{\pi}(i_1 + i_2)\sin\theta d\theta \; I = \frac{\lambda^2}{4\pi}\int_0^{\pi}(i_1 + i_2)\sin\theta d\theta$$

where i_1 is the intensity scattered in the θ direction by a single isotropic sphere from an incident polarized beam with electric vector perpendicular to the plane of observation and i_2 is the intensity in the plane of observation. For spherical particles, intensity includes Riccati—Bessel functions and size parameters k_a, where $k_a = 2\pi / \lambda$ and α is the particle radius.

4. Volume Scattering Function

Since it plays a key role in the theory of radiative transfer, the volume scattering function is the most important inherent property for the understanding of optical oceanography. Volume scattering β(θ) describes the probability that a photon will be scattered at an angle θ (measured from the forward direction) after scattering in a volume of water. The larger the value of β(θ) is, the faster the beam disperses.

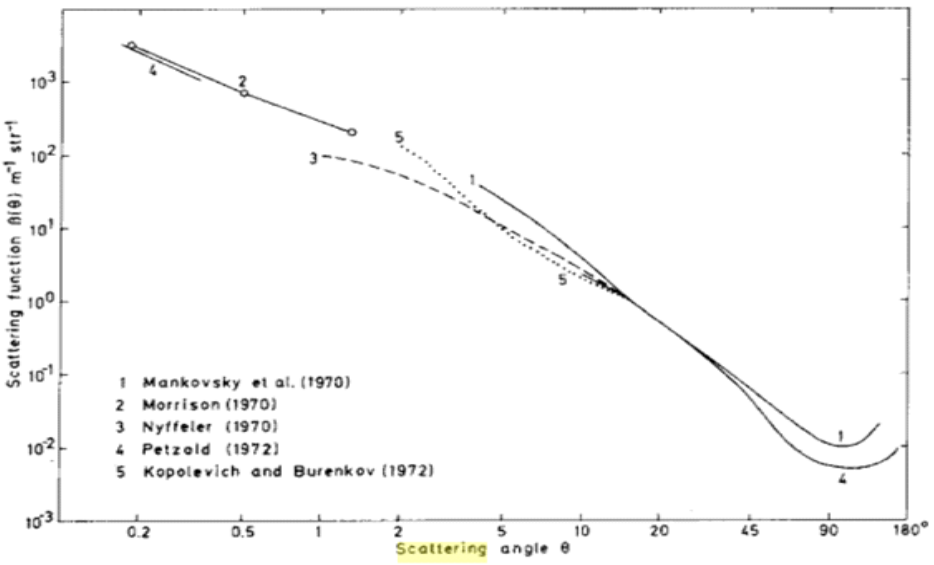

Figure 4. Comparison between different normalized volume scattering functions of ocean water as a function of the scattering angle θ. (From [3])

5. Dispersion of Scattering

Scattering has a wavelength selectivity, which is mainly attributed to three factors: Scattering by water itself; scattering by small-sized particles ; and absorption by particles. This selectivity can be seen from equation (3.1) and the λ^4 factor for Rayleigh scattering.

6. Multiple Scattering

Multiple scattering is the irradiation of the each water volume element, not only by the original beam, but from light scattered from previous elements as well. Thus, the light is scattered several times. This effect is highly dependent on the particle concentration, the size of the volume and the attenuation factor. For small volumes and low particle concentration, multiple scattering is considered negligible.

E. ATTENUATION OF SEA WATER

The combined action of absorption and scattering results in the attenuation process inside the sea water. The important parameter describing this phenomenon is the total attenuation coefficient c, which is the sum of the scattering and the absorption coefficients. Attenuation is due to particles and due to absorption of dissolved organic substances. Sea salt has little effect on water attenuation.

Attenuation is primarily an absorption that depends on wave length. In the infra red region, scattering can be completely neglected compared to absorption. Generally, absorption tends to increase with increasing wavelength, as shown in Figure 5. This relationship is attributed to several infrared absorption bands.

The absorption coefficient, a(λ), is a measure of the conversion of radiant energy to heat and chemical energy. It is numerically equal to the fraction of energy absorbed from a light beam per unit of distance traveled in an absorbing medium. Its dependence on the wavelength is shown in Figure 5.

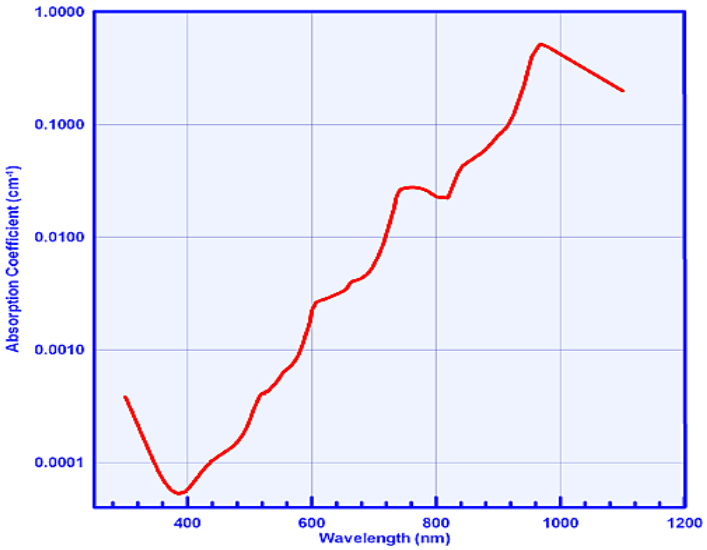

Figure 5. Absorption coefficient α as function of wavelength (From [1])

When dealing with attenuation from particles, however, the wave length dependence is different. Attenuation tends to increase exponentially at shorter wavelengths, as shown in Figure 6. Even if scattering demonstrates wave length selectivity as discussed before, the main contribution to the selective effect is due to absorption.

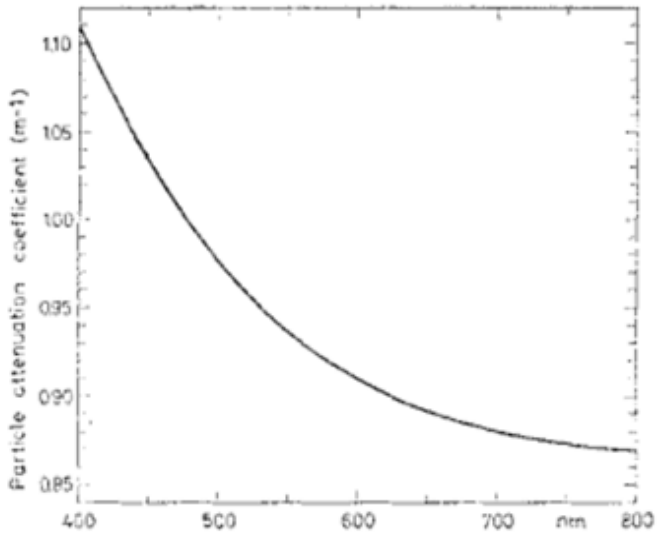

Figure 6. Particle attenuation coefficient as a function of the wavelength (From [3])

THIS PAGE INTENTIONALLY LEFT BLANK

III. SIMULATING THE OCEAN SURFACE

This chapter introduces some of the background knowledge and concepts required for understanding wind-generated ocean surface models.

A. THEORETICAL APPROACH

A statistical description of wind-generated surface waves is very important for examining the effects of the laser propagation through the ocean surface. Much work has been devoted to the study of the statistics of the ocean surface. In 1953, Cox and Munk studied sun glitter on the ocean surface using aerial photography. Oceanographers Pierson and Moskowitz developed spectral density functions and analytical solutions for the height variance of the ocean surface versus wind speed. Their model was later improved by the North Sea Wave Project (JONSWAP) spectrum. Elfouhaily, Katsaros and Chapron refined this model to enhance wind effects for small scale waves.

Regardless of the means of construction, a wave spectrum must agree with observations, as well as satisfy certain criteria. These criteria include a dependence on fetch conditions. In the high-frequency region, the wind - dependent mean-squared slope should agree with observations made by Cox and Munk.

1. Cox and Munk Results

Since these measurements are the basis for evaluating various ocean spectrum models, the results obtained by Cox and Munk are presented first.

Combining aerial photography of the sun’s glitter on the sea surface in Hawaiian sea and measurements of wind from a vessel provided the following results regarding the slope distribution of the surface. Cox and Munk showed that the slope variance (mean-squared slope), regardless of direction, increases linearly with wind speed [4].

$$\sigma_c^2 = 0.003 + 1.92 \times 10^{-3} U_{19.5}$$
$$\sigma_u^2 = 3.16 \times 10^{-3} U_{19.5}$$
$$\sigma_c^2 + \sigma_u^2 = 0.003 + 5.12 \times 10^{-3} U_{19.5}$$

where σ_c^2 and σ_u^2 correspond to the cross and up wind components of the mean-squared slope. $U_{19.5}$ represents the wind speed 19.5 m above the ocean surface. The above linear dependence is seen in Figure 7. The Cox Munk results have become the reference criteria for testing the validity of an ocean wave slope measurement.

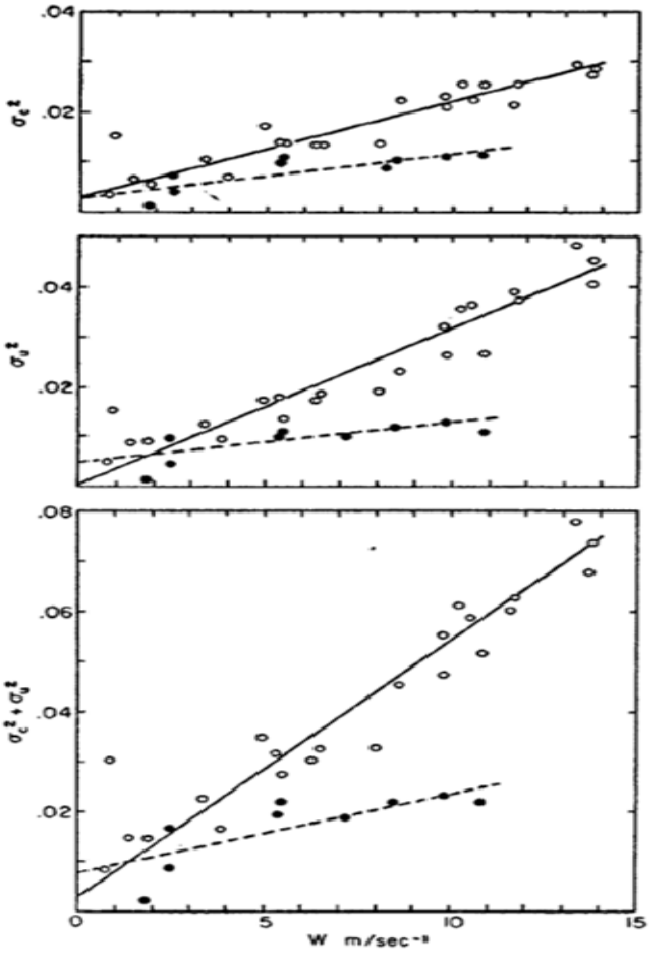

Figure 7. Mean-squared slope and their components as a function of the wind speed. (From [4])

2. Pierson-Moscowitz Spectrum

The Pierson-Moscowitz Spectrum has the advantage of being simple, reasonably close to actual ocean spectrum, particularly for long waves. It is a good starting point for examining the various models. It assumes a fully developed sea (a sea produced by winds that blow steadily for a long period of time over a large area), meaning that a large (>18 km) fetch exists. One critical benefit is that the Pierson-Moscowitz Spectrum has a known analytical variance and surface slope spectrum. The ocean surface wave power spectral density for a fully developed ocean is given by [5]

$$S(\omega) = \frac{\alpha g^2}{\omega^5} \exp[-\beta(\frac{\omega_0}{\omega})^4] \tag{2.1}$$

In this expression, α = 0.0081, β = 0.74, $\omega_0 = \frac{g}{U}$ $\omega_0 = \frac{g}{U}$, where g is the acceleration of gravity and U is the wind speed at 19.5 m above the surface. The angular frequency $\omega = 2\pi f$, where f is the wave frequency in Hz, in Eq. (1.1) is defined for positive frequencies only.

To depict the ocean surface in spatial coordinates, the Pierson-Moscowitz Spectrum has to be rewritten in terms of the wave number k. Using the deep water dispersion relationship

$$\omega^2 = gk \tag{2.2}$$

and

$$S(k) = S(\omega)\frac{d\omega}{dk} \tag{2.3}$$

the wave number spectrum is then in one dimension

$$S(k) = \frac{\alpha}{2k^3} \exp[-(\frac{\beta g^2}{k^2 U^4})] \tag{2.4}$$

Equation (1.4) is defined for positive k only. Integrating either Eq. (2.1) or Eq. (2.4) over ω or κ gives the variance of the ocean surface wave as

$$\sigma^2 = \frac{\alpha}{4\beta}\frac{{U_{19.5}}^4}{g^2} = 0.00274\frac{{U_{19.5}}^4}{g^2} \tag{2.5}$$

In two dimensions, a directivity factor is needed to compensate for the lack of isotropy with respect to waves in the direction of wind and perpendicular to the wind direction. The two dimensional directivity factor is given by

$$D(k,\varphi) = \frac{\cos^2\varphi}{\pi} \tag{2.6}$$

The 2D spectrum has the form $$S(k) = \frac{\alpha}{2k^4}\exp[-(\frac{\beta g^2}{k^2U^4})]D(k,\varphi) \tag{2.7}$$

The elevation spectrum for wind speeds 2-20 is presented in Figure 8.

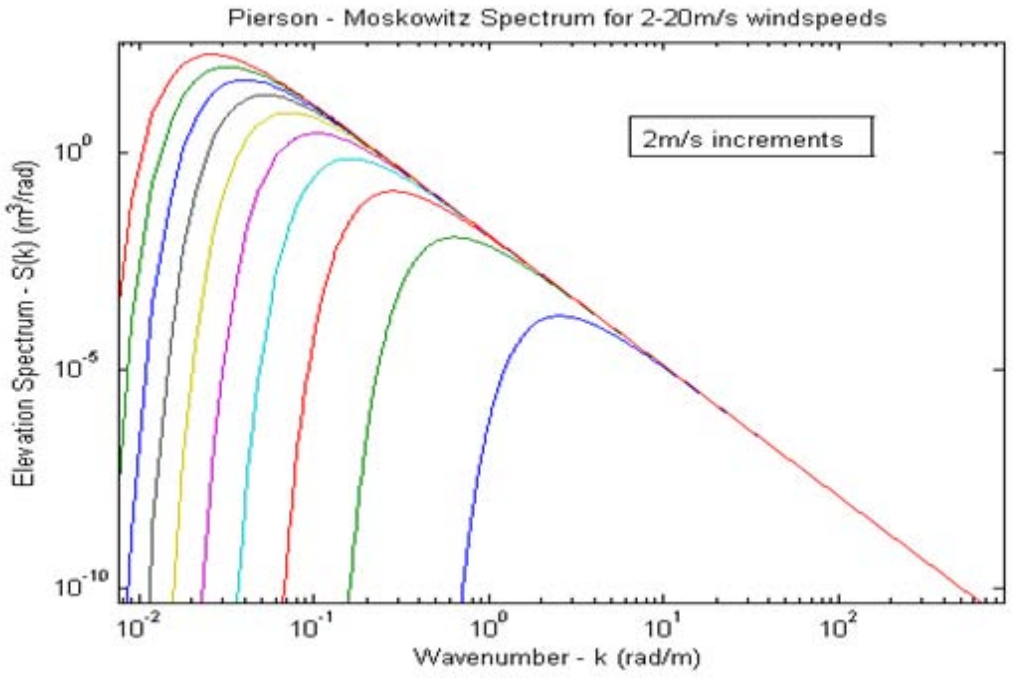

Figure 8. Pierson-Moskowitz 1-D Elevation Spectrum for different wind speeds as a function of the wave number k

3. Simulating Ocean Waves with Pierson-Moskowitz Spectrum

To simulate ocean surface waves, a Fourier Transform of Equation (2.4) will give the autocorrelation function of the ocean surface waves. This method does not give the amplitude versus spatial coordinates. One way to perform the numerical simulation is to filter Gaussian random noise in spatial coordinates using the square root of Equation (2.4) and inverse Fourier Transforming this filtered spectrum to spatial coordinates. A more detailed synopsis of the procedure required can be presented by the following steps:

- *Start with an 1-D array of Random Gaussian*
- *Fourier Transform this Array in Frequency Coordinates*
- *Filter this Spectrum with the Pierson-Moscowitz Spectrum*
- *Inverse Fourier Transform Back to X Coordinates*
- *Scale the Results to Correct for 1/N Factors*

The Matlab code for generating a numerical simulation of the ocean surface using the Pierson-Moskowitz Spectrum is code A in Appendix B.

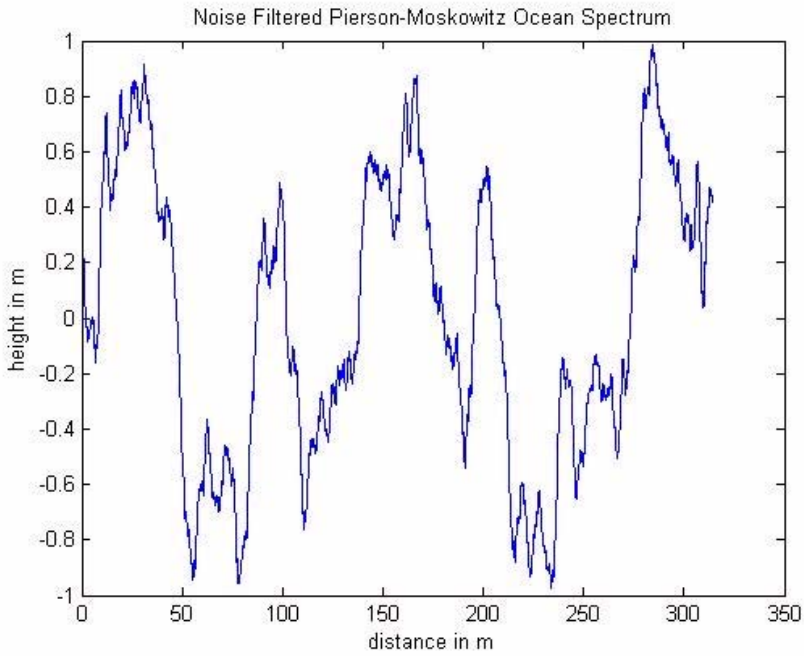

Figure 9. Noise filtered, 1D, Pierson-Moskowitz Spectrum as a function of distance

4. PM Spectrum Mean-Squared Slope

One problem with the Pierson-Moskowitz Spectrum is that it underestimates the high frequency components of the spectrum. These short waves, also known as capillary waves, have an important contribution to the mean-squared slope of the surface. This behavior can be observed from Figure 10, where the κ^{-3} dependence is obvious.

As described previously, a wave spectrum must be capable of providing agreement with the Cox and Munk results regarding the mean-squared slope. The Pierson-Moskowitz Spectrum diverges logarithmically as the wave number gets bigger. This is due to the κ^{-3} dependence. Analytically, this can also be confirmed. The mean-squared slope is obtained by integrating the spectrum Eq. (2.4) over all wave numbers κ as follows [6]

$$S_L^2 = \int_{-k}^{k} S(k)k^2 dk = -(\frac{\alpha}{4})\exp\mathrm{int}(-\frac{\beta g^2}{k_c^2 U^4}) \tag{4.1}$$

where κ_c is the cut off wave number.

As shown in Equation (2.4), S(k) has an $\frac{1}{\kappa^3}$ dependence. Substituting in Eq.(4.1) inside the integral retains the $\frac{1}{\kappa}$ factor. Our initial equation has now become $\int_{-k}^{k} \frac{1}{k} dk$. This integral finally gives us the mean-squared slope $\ln k_{-k}^{+k}$.

As wave number k increases, the mean-squared slope will diverge, reaching infinite values. This is not physically observed. Ocean waves cannot have infinite slope. Using the numerical simulation of the Pierson-Moskowitz Spectrum, the results are the same. Increasing the number of data points in the simulation, the mean-squared slope constantly increases. This is without saturating to a specific value. Although this spectrum is suitable for examining the low frequency region (large waves) and has an analytical form to calculate the mean-squared slope, it does not fall off fast enough at high frequencies.

5. JONSWAP Model

The JONSWAP spectrum was developed for the North Sea oil fields. It assumes that a wave spectrum is never fully developed, but keeps developing through non-linear, wave interactions for long distances and for long periods of time. To apply this theory, the JONSWAP spectrum has a spectral peak enhancement factor J_P included in the Pierson-Moskowitz Spectrum. This factor improves the spectrum's accuracy at low frequencies by including the wave age. The problem, however, with the high frequency waves remains. The JONSWAP factor is given by [7]

$$J_P = \gamma^{\Gamma}, \tag{6.1}$$

where

$$\gamma = 1.7 \text{ for } 0.84 < \Omega < 1 \text{ and}$$

$$\gamma = 1.7 + 6 \ln(\Omega) \text{ for } 1 < \Omega < 5$$

and

$$\Gamma = \exp\left[\frac{-\left(\sqrt{\frac{\kappa}{\kappa_p}} - 1\right)^2}{2\sigma^2}\right. \tag{6.2}$$

where $\sigma = 0.08\,(1 + 4\Omega^{-3})$. The inverse wave age Ω is defined as

$$\Omega = 0.84 \tanh^{-0.75}\left(\frac{X}{X_o}\right)^{0.4} \tag{6.3}$$

X_0 is a fetch constant and has the value X_0 =22000 m and the non -dimensional fetch $X = \frac{gx}{U_{10}^2}$, where x is the dimensional fetch, x = 10^6 m.

An improved spectrum that includes more data at the high frequency region is, consequently, more suitable for this study's purpose. This improved spectrum will be presented next.

6. Elfouhaily Model

The model proposed by Elfouahily [8] is valid for a larger range of frequencies and addresses the higher frequency waves. Furthermore, it agrees both with Cox Munk data and the Pierson-Moskowitz analytical results. The Elfouahily model is more satisfactory for this study's approach. In 1-D, the Elfouahily model has two spectral regions as follows [8]

$$S(\kappa) = \frac{1}{\kappa^3}[B_l + B_h] \tag{7.1}$$

where B_h and B_l express the high and the low frequency curvature spectrum. The total curvature spectrum is expressed as $B = \kappa^3 S$ in order to remove the κ^{-3} dependence of the elevation spectrum, observed in the previously discussed models. The rate of change of the ocean surface slope can be approached by plotting the spectrum as a function of the wave number k as presented in Figure 10. The effect of high frequency waves is included. After the value k=300 rad/m, the spectrum falls off very fast. This prevents the integral of the spectrum from diverging.

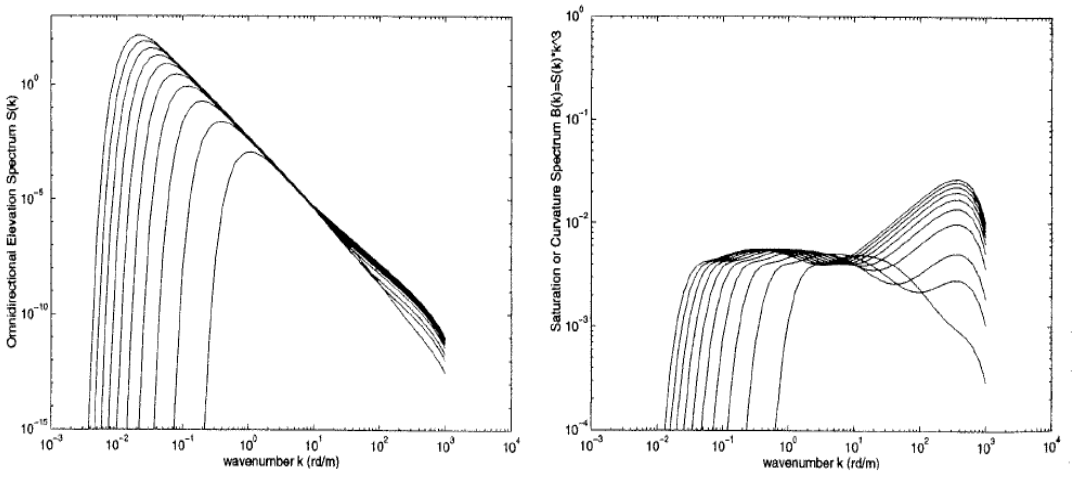

Figure 10. The Elfouhaily 1D Elevation spectrum S(k) and the corresponding curvature spectrum B(k) as a function of the wavenumber k for different wind speeds. (After [8])

The low frequency term (long wave curvature spectrum) is defined as

$$B_l = \frac{a_p}{2} \cdot \frac{c_p}{2} \cdot L_{PM} \cdot J_p \cdot \exp[-\frac{\Omega}{\sqrt{10}}(\sqrt{\frac{\kappa}{\kappa_p}} - 1)] \tag{7.2}$$

where a_p is the Phillips-Kitaigorodskii equilibrium range parameter for long waves and is given by $a_p = 0.006\sqrt{\Omega}$, with Ω the dimensionless inverse wave age parameter defined in Equation (6.3). The phase speed at spectral peak c_p is defined as

$$c_p = \sqrt{\frac{g}{\kappa_p}} \tag{7.3}$$

where the wave peak wave number k_p is given by $\kappa_p = \kappa_0 \cdot \Omega^2$ and $k_0 = \frac{g}{U^2}^2$.

L_{PM} is the Pierson-Moskowitz spectral shape and is given [8] by

$$L_{PM} = \exp[-\frac{5}{4}(\frac{k_p}{k})^2] \tag{7.4}$$

The high frequency term in Eq. (6.1) is given by [8]

$$\mathrm{B}_h = \frac{\alpha_m}{2} \cdot \frac{c_m}{c} \cdot \exp[-\frac{1}{4}(\frac{\kappa}{\kappa_m} - 1)^2] \tag{7.5}$$

where c_m is the Capillary peak celerity and has the constant value c_m=0. 23 m/sec. κ_m is the Capillary peak wave number and has the value κ_m=361.4/m.

To define the parameter α_m (analogous to equilibrium range parameter in the low frequency spectrum), the friction velocity u^* has to be defined as [8]

$$u^* = \frac{0.42 \cdot U_{10}}{\ln \frac{10}{z_0}} \tag{7.6}$$

where z_0 is the roughness length and is given by

$$z_0 = 3.7 \cdot 10^{-5} \cdot (\frac{U_{10}{}^2}{g}) \cdot (c_p U_{10})^{0.9} \tag{7.7}$$

The above equation found in [8] cannot be correct. Checking the units for the roughness length, it is concluded that the correct form has to be

$$z_0 = 3.7 \cdot 10^{-5} \cdot (\frac{U_{10}{}^2}{g}) \cdot (\frac{U_{10}}{c_p})^{0.9} \tag{7.8}$$

in order to get meters as a result. Now the parameter α_m is defined as

$$\alpha_m = 0.01 \cdot [1 + \ln(\frac{u^*}{c_m})] \text{ for } u^* < c_m$$

$$\alpha_m = 0.01[1 + 3\ln(\frac{u^*}{c_m}) \text{ for } u^* > c_m$$

As seen by comparing equations (7.2) and (7.5), the Pierson-Moskowitz spectral shape is only contained in the low frequency curvature spectrum. To address the high

frequency waves, however, this low frequency roll-off term has to be applied in both spectral terms. Without this term, the Elfouhaily model would diverge at low frequencies. This is because the high frequency curvature spectrum B_h interacts with all wave numbers. Without including a Pierson-Moskowitz roll-off the spectrum cannot go to zero. Since the waves would have infinite height at low frequencies, this cannot be a physical consequence.

B. COMPUTER SIMULATION

After deciding upon a spectrum model, this study's researchers determined that the mean-squared slope of the Elfouhaily Spectrum must be compared with the Cox Munk results. This model will be presented in the third part of this thesis, where the Snell's Law will be applied in an ocean surface.

1. Agreement with Observations

Although the Elfouhaily Spectrum provides a result with a physical meaning, it was found that it did not agree with the Cox-Munk results, as indicated in Figure 11. Furthermore, it was observed that the two methods used for slope calculations in the code B seemed to deviate from each other, giving slightly different results. The third observation, which seems not to be in order, is a discontinuity that exists in the graph linearity, especially in high winds. Figure 11 shows the mean-squared slope versus wind speed, both for slope 1 and slope 2.

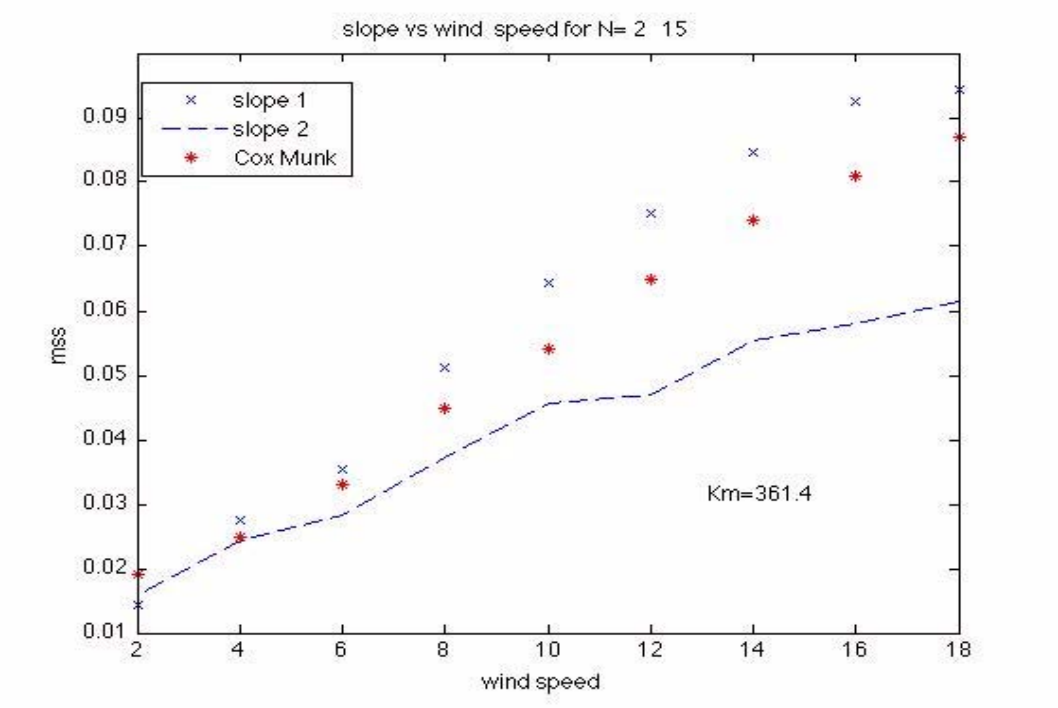

Figure 11. Slope 1 and 2 of the Elfouhaily Spectrum as a function of the wind speed compared to the Cox Munk results.

2. Dependence on the High Frequency Cut Off

Since the results of this study's model were not satisfactory, changes were applied. A first look indicates that the model works well in low wind speeds, but, as the wind increases, there is a significant deviation from Cox and Munk results. To make the simulation more realistic, the high frequency limit was first increased by increasing the number of data points. The difference between the two slopes disappeared. In Figure12, this result is presented using 2^{20} data points for the FFT spectrum.

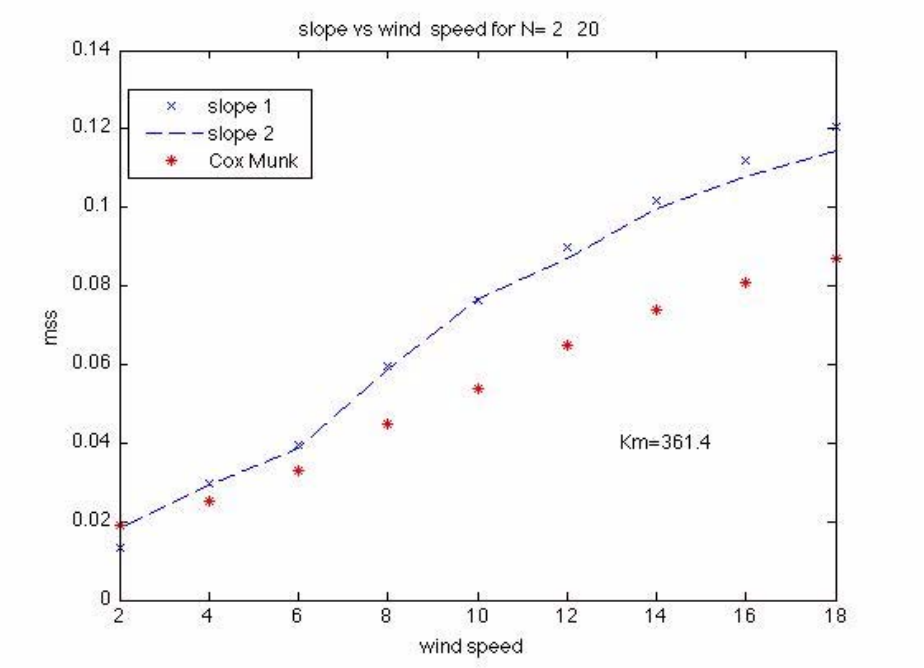

Figure 12. Slopes 1 and 2 of the Elfouahily Spectrum as a function of the wind speed compared to the Cox Munk results

3. Changing the Capillary Peak Wave Number

The capillary peak wave number k_m is a function of the water density ρ, the gravitational constant g and the ocean surface tension T. It determines the sharp roll off of the Elfouahily Spectrum at high frequencies. It is given by

$$k_m = \frac{\rho g}{\mathrm{T}}$$

and, as stated before, has the value of 361.4(rad /m).

Field measurements of intermediate scale waves by Hwang [9], however, showed different results. The observed peak occurs at much lower wave numbers than the above constant. Furthermore, k_m is not constant, but depends on wind speed. This data is presented in Figure 14.

The area under the curve in a range of wave numbers corresponds to the mean-squared slope, since $B(\kappa) = \kappa^3 S(\kappa)$. The calculated slopes are in agreement with those

obtained from [4]. Observing the peak of the distribution of the mean-squared slopes represented by $B(\kappa)$ allows the estimation of a more realistic value for capillary peak wave number in the simulation code.

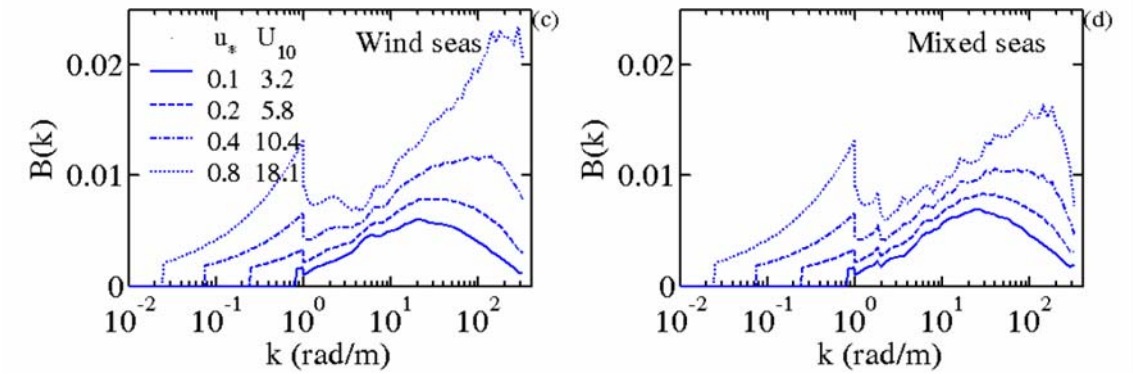

Figure 13. Curvature spectrum measured by Hwang as a function of the ocean wave number k (From [9])

As can be seen, the peak of the spectrum for various wind speeds appears, at a maximum, in ranges from 20 rad/m to 200 rad/m. Making different trials in the simulation code and comparing the graphic results with the corresponding Cox Munk data, these researchers selected the value of 160 rad/m for Km. The mean-squared slope graph can be seen in Figure 14. It can now be seen that, for smaller wind speeds, the corresponding data almost overlaps, demonstrating that the Elfouhaily model spectrum is appropriate for these wind speeds. For stronger winds, however, there seems to be only a small deviation.

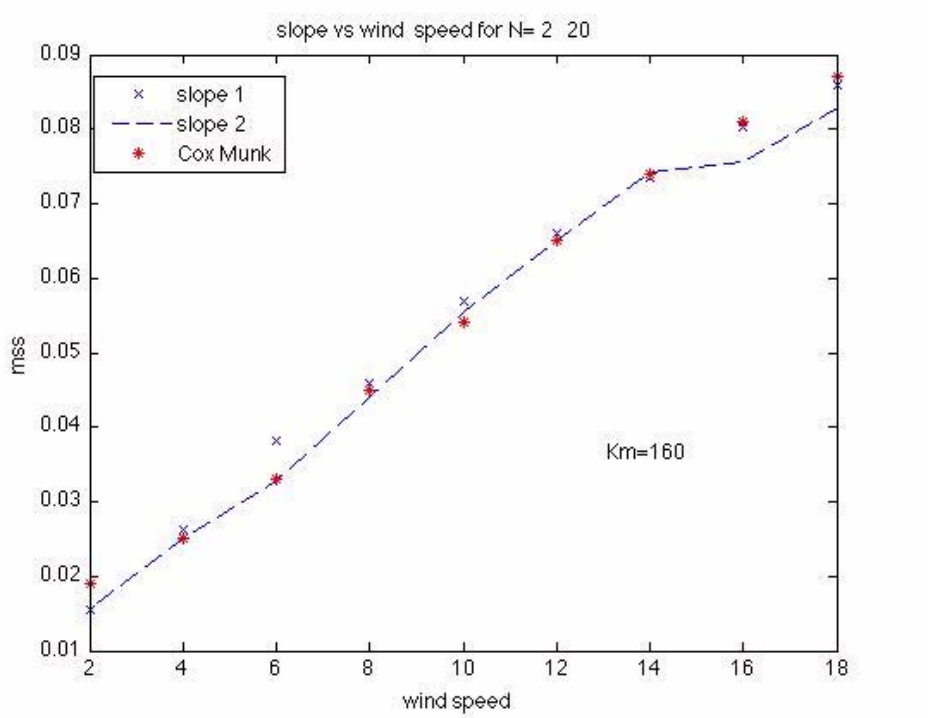

Figure 14. Slopes 1 and 2 of the Elfoyhaily Spectrum compared to the Cox Munk results for Km = 160

4. Capillary Peak Wave Number as a Function of Wind Speed

Taking again into consideration Hwang's results, these researchers considered the relation between capillary peak wave number and speed. Hwang showed that k_m shifts upward with increasing wind speed. Analyzing the data that corresponded to the peak of the spectrum for each used wind speed from figure, the results ended in a linear relationship between the two parameters

. $$k_m = 0.077872k - 31.797 \quad (4.1)$$

Substituting this relationship in this study's code and running again the simulation, the results are shown in Figure 15. A good agreement with the desired results appears in the higher wind speeds and an approach that is satisfactory at lower speeds. Furthermore, there is no discontinuity in the graph's linearity, something that was common for a fixed capillary wave spectral peak.

The poor agreement, seen in Figure 15 at low frequencies, suggests that a quadratic dependence on U may be more appropriate than the linear dependence used in equation (4.1).

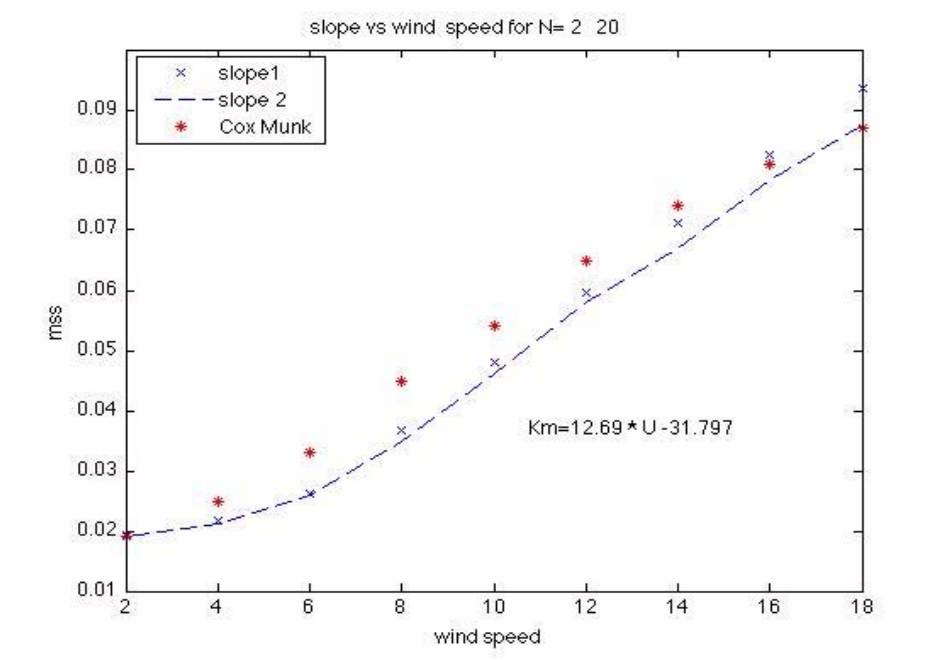

Figure 15. Slopes 1 and 2 of the Elfoyhaily Spectrum as a function of the wind speed compared to the Cox Munk results, using the relationship Km = 12.69 U -31.797

C. CHAPTER SUMMARY

In this chapter, two different ocean spectrums were used to generate a mathematical model for a wind-generated ocean surface. Initially, the Pierson-Moskowitz Spectrum was examined, but rejected since the corresponding mean-squared slope diverged at high frequencies. Next, the Elfouhaily Spectrum was tested. Although more complicated, it did agree with physical results, having a non diverging mean-squared slope. The agreement with measured observations was then evaluated. After altering specific parameters in the mathematical approach and computer simulation, an ocean surface model was constructed that agreed with Cox Munk observations, a fact that reinforces its validity and suitability for this study's purpose.

IV. SIMULATION AT THE AIR WATER INTERFACE

A. GEOMETRICAL OPTICS' APPROACH

This section develops a geometrical optics' model to examine the effects of light entering or leaving a water surface. The ocean model discussed in Chapter III was used. To generate a physically accurate ocean surface from this model, this study followed the same procedure as described in paragraph II-3. White noise was filtered with the wave number spectrum. The final outcome was the ocean slope distribution. The incoming light ray interacts with this slope, refracting according to the Snell's Law and exiting with a new angle. The corresponding code is in the Appendix.

1. Snell's Law

The simulation geometry is as follows: A light ray γ_2 is incident on the water surface with corresponding angle γ_1 to the normal. The ray exits with angle γ_2. The local ocean slope is R. By Snell's Law we have

$$n_1 \sin\gamma_1 = n_2 \sin\gamma_2 \tag{1.1}$$

where $n_1 = 1.33, n_2 = 1$ are the corresponding indices of refraction for water and air.

Figure 16 represents the geometry of the simulation.

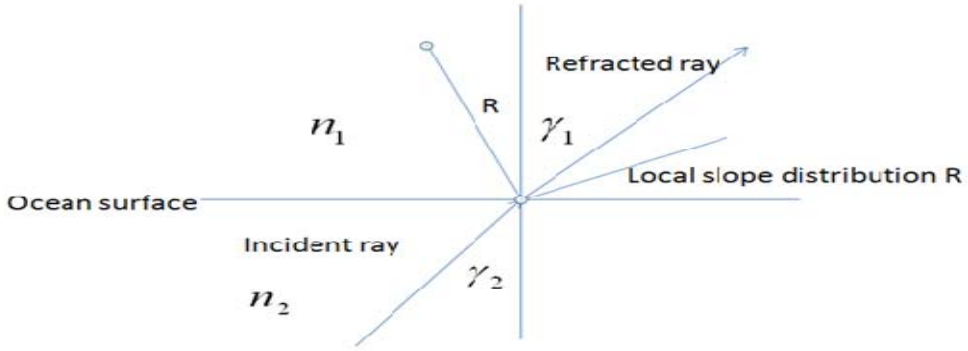

Figure 16. Geometry Simulation for applying Snell's Law in an ocean surface with slope distribution R (After [10])

Solving for γ_1, we get [11],

$$\gamma_1 = \sin^{-1}[\frac{n_1}{n_2}\sin(\gamma_2 + R)] - R \qquad (1.2)$$

.

This relationship applies to the laser light distribution just beneath the boundary and is valid for light both entering and exiting the ocean surface. The entering and exiting angles are always defined with respect to the vertical.

2. Assumptions

The scattering and absorption effect will be initially neglected and examined in the following chapter. Scattering includes both the initial interference and the following multi-scattering phenomena. Wave obscuration of the optical rays is also neglected. Propagation is assumed to be vertical and the ocean angular variance R is small.

3. Analytical Solutions

From [11], the variance of the ray angle after penetrating the sea surface is given approximately by

$$\mathrm{var}[\gamma_1] \simeq \left|1-\frac{n_1}{n_2}\right|^2 \mathrm{var}\left[R\right] \tag{3.1}$$

and

$$\frac{\mathrm{var}\left[\gamma_1\right]}{\mathrm{var}\left[R\right]} = \left|1-\frac{n_1}{n_2}\right|^2 \tag{3.2}.$$

Calculating the $\left(\frac{d\gamma_1}{dR}\right)$ from equation [1.2] with respect to R results in

$$\left(\frac{d\gamma_1}{dR}\right) = \left|\frac{n_1}{n_2}\frac{\cos(\gamma+\langle R\rangle)}{\sqrt{1-\left(\frac{n_1}{n_2}\right)^2 \sin^2\left(\gamma_2+\langle R\rangle\right)}}-1\right| \tag{3.3}$$

Squaring the result and multiplying by the variance of the local slope R gives a better approximation of the variance of the refracted angles.

$$\mathrm{var}\left[\gamma_1\right] = \left(\frac{d\theta}{dR}\right)^2 \mathrm{var}\left[R\right] \tag{3.4}$$

4. Simulation

The simulation was written in Matlab and code C and it appears in Appendix. Local slope R is determined from the Elfouhaily Spectrum and was calculated with simulation code. The output is shown in Figure 17, which demonstrates the ratio of variances versus the incident angle.

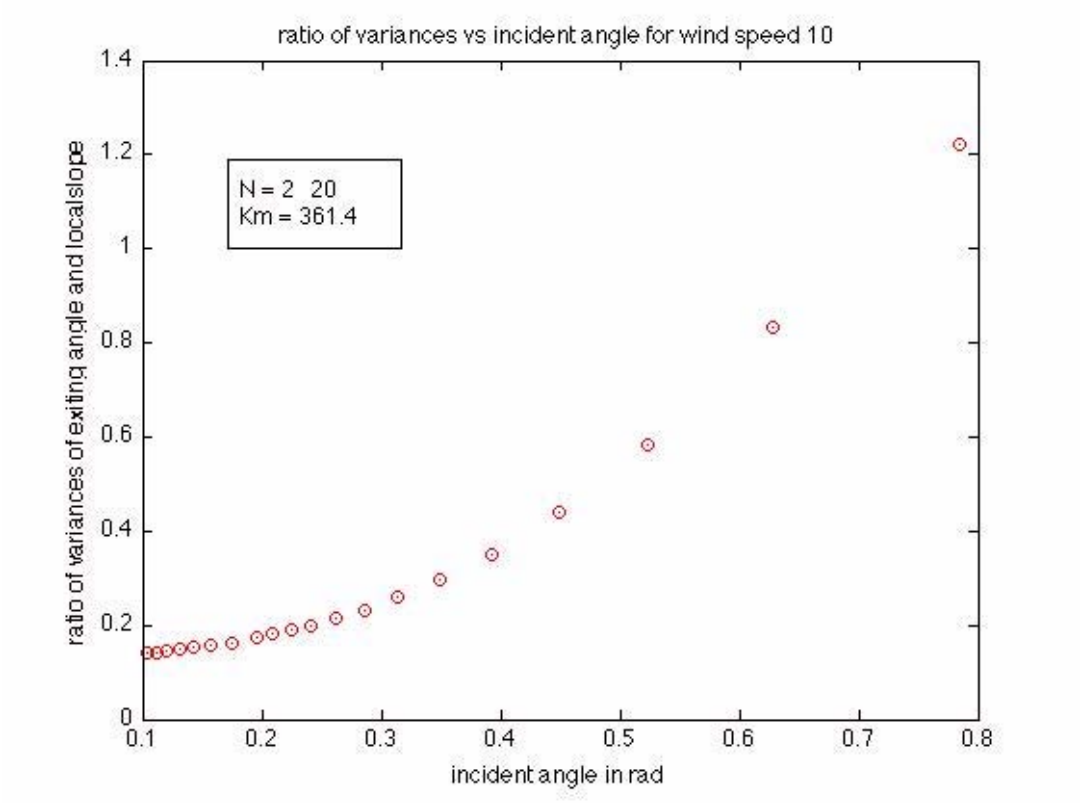

Figure 17. Variance of ratio of exiting angle and local slope versus incident angle

B. CHAPTER SUMMARY

This chapter used Snell's Law to determine the distribution of refracted waves versus wind speed to the ocean surface model generated in the previous chapter. A geometric optics' approach was used. Scattering and absorption during light's penetration in the water body were ignored. Examining the ratio of variances of the exiting angle and the local slope, it was shown that the refractive effects of the ocean surface were relatively small.

V. THEORY OF RADIATIVE TRANSFER IN THE SEA

The complex behavior of the photons inside a water body, from the simultaneous effects of absorption and scattering and the shape of the volume scattering function, prevents the establishment of an analytical relationship between the apparent and the inherent optical properties. Monte Carlo Computer simulation techniques can provide a description of the scattered underwater light field, given the measured optical properties of the water and the characteristics of the incident radiant flux.

A. MONTE CARLO SIMULATION OF LIGHT PENETRATION INTO NATURAL WATERS

Although the sea's inherent optical properties that determine the light behavior inside water may be known, there is no analytical means to predict the photons' movement in a scattering medium. Thus, the underwater light distribution field cannot be determined directly.

These optical properties, however, do provide useful information. They inform us of all the possible ways a photon can move, the possible interactions with the scattering medium and the corresponding probabilities of the above. A photon can be absorbed in a specific path length or scattered in a specific path length and at a specific angle. Using suitable computer simulation techniques, for given values of inherent properties, the corresponding apparent ones and other parameters of the underwater light field have been calculated by Kirk.

This is the idea behind the Monte Carlo simulation where the movement of a large number of photons is calculated in the computer and the average photon flux is calculated. The code implemented by Kirk using Monte Carlo simulation was used for the scope of this thesis. A brief synopsis is provided next.

1. Kirk Code

Reflection from the surface was ignored. The water surface was considered flat and only the direct light beam was taken into consideration. The water body was assumed to have finite depth. The objective was to estimate the nature of light field at each depth.

Just below the surface and after refraction, a photon's trajectory is determined by its angle α with respect to the horizontal given by

$$\alpha = \arccos[(\cos\alpha^*)/1.33] \quad , \tag{1.1}$$

where α^* is the light altitude. The probability of the photon moving at a specific distance before its first interaction is determined by the attenuation coefficient c. A random number r between 0 and 1 is selected and the corresponding path length is [12]

$$P = -(\frac{1}{c})\ln(1-r) \tag{1.2}$$

Psin(α) gives the corresponding depth . A new random number decides the nature of the interaction. For absorption, a new photon enters the water and the procedure continues. Scattering requires a new scattering angle θ (angle between photon's trajectory before and after scattering) and rotation angle φ (angle of rotation of the new trajectory around the previous one). The probability that a photon may be scattered at an angle θ is given from the volume scattering phase function β(θ). A new random number is assigned a value of scattering angle θ from the cumulative distribution. The water had a normalized volume scattering function β(θ), which is the same as the experimental measurements of Petzold in San Diego Harbor. A subsequent random number provides the rotation angle φ. The new angle α′of the photon relative to the horizontal is now [12]

$$\sin a' = \sin a\cos\theta + \cos a\cos\varphi \tag{1.3}$$

where α is the angle calculated in the previous step. Before the next interaction and the corresponding depth, a new random number determines the path length.

When the movements of all photons are calculated, the total photon flux at each depth provides a measure of the downward or upward radiance. The other quantities

provided as outcome from this program are the average vertical attenuation coefficient, average cosine and radiance distribution in each depth , the x, y coordinates and the θ, φ angles for each photon.

The above calculation applies to monochromatic radiation only.

2. Testing the Kirk Code

To validate the Monte Carlo code and to provide useful and reliable results, the results should agree with known measurements, as in Chapter III, which compared Elfoyhaily model to the Cox Munk results. The code results were initially compared to measured values of irradiance attenuation coefficient for given values of solar elevation, wavelength, scattering and absorption coefficients. The input values used were the same as in Table 10 from [3]. Table 15 from [3] provided the scattering coefficient data. The depth interval between layers of 1m was used in the program according to the measurements. The code results are very close to the measured ones, as indicated in Tables 1 and 2.

The second comparison included the irradiance attenuation coefficient from [13]. This was for the same given scattering parameters and scattering function. The only difference was that a constant solar angle of 90 degrees and a depth interval of 0.1 m were used. Because of the high scattering attenuation, the code results were very accurate.

Both comparisons proved to be very close to the observed values and so validated the code.

Wavelength λ (nm)	**Absorption coefficient α (m^{-1})**	**Scattering coefficient β (m^{-1})**	**Irradiance attenuation coefficient E_K (m^{-1})**	**Irradiance attenuation coefficient E_K (m^{-1}) *calculated by Kirk Code***
200	3.07	0.151	3.14	3.08
300	0.141	0.0262	0.154	0.141
400	0.0171	0.0076	0.0209	0.017
500	0.0257	0.0029	0.0271	0.026
600	0.244	0.0014	0.245	0.244
700	0.650	0.0007	0.650	0.649
800	2.07	0.0004	2.07	2.06

Table 1. Comparison between observed values of the Irradiance attenuation

Region	**Solar elevation in degrees**	**Wavelength λ (nm)**	**Absorption coefficient α (m^{-1})**	**Scattering coefficient β (m^{-1})**	**Irradiance coefficient $K_E = \frac{\mu}{\alpha}$ (m^{-1})**	**Irradiance coefficient *calculated by Kirk Code***
Mediterranean Sardenia	72	372	0.058	0.05	0.07	0.06
Mediterranean Sardenia	74	633	0.29	0.05	0.31	0.30
Baltic	52	372	0.97	0.2	1.22	1.11

Baltic	48	633	0.33	0.2	0.42	0.40
Baltic	52	535	0.09	0.2	0.12	0.118

Table 2. Comparison between observed values of the Irradiance attenuation coefficient and results derived from the Monte Carlo simulation

B. SIMULATION RESULTS

Running the Kirk Code for various input values of both absorption and scattering coefficients provided a measure of the effect of these parameters for light distribution within the ocean. The ocean water body was divided into 21 depth layers. After the 21st layer, the scattered photon distribution, starting from the initial point focused laser beam, interacted with the local slope ocean surface from the Elfouhaily model using Snell's Law .This gave the final distribution of the photons as they exit the surface.

An initial photon elevation angle of 90 degrees and a depth interval of 10m were used throughout the simulation.

The original code was written [12] in FORTRAN 77 and was translated into FORTRAN 95 by Professor Walters. This translation was done to avoid the many 'go to statements and back references.'

Three cases were examined independently. In the first case, named I, very small values of the absorption and scattering coefficient were chosen. These corresponded to negligible effects of the absorption and scattering phenomena. Next, in case II, higher values were selected to examine the relationship of the above parameters with the light distribution inside the water when the above phenomena are significant. Finally, the last case, named III, considered intermediate values of the absorption and scattering coefficients. This was mainly to test and confirm that there is a logical and expected relationship between the light distribution and the laser footprint and the variation of the inherent optical properties.

In each case, two 3D graphs of the eleventh and twenty-first layers were presented. The last one is the most important. This is because it describes the light distribution just before the interaction with the ocean surface. For better understanding of the laser footprint size and shape, a 2D graph of the twenty-first layer is also provided.

1. Case I (Small Extinction)

For this case, the following values will be assigned to the input parameters:

Absorption coefficient a = 0.01 1/m

Scattering coefficient b = 0.01 1/m

Depth interval = 1 m for a total depth of 21 m

Photon angle in the water = 90 degrees

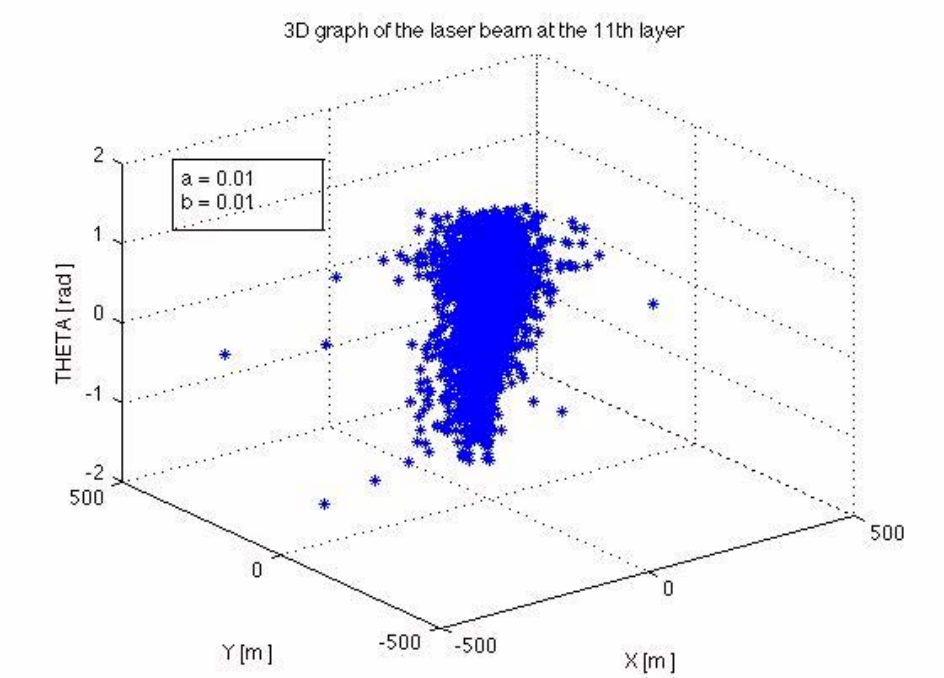

Figure 18. Light distribution at the eleventh layer for case I for 10 m

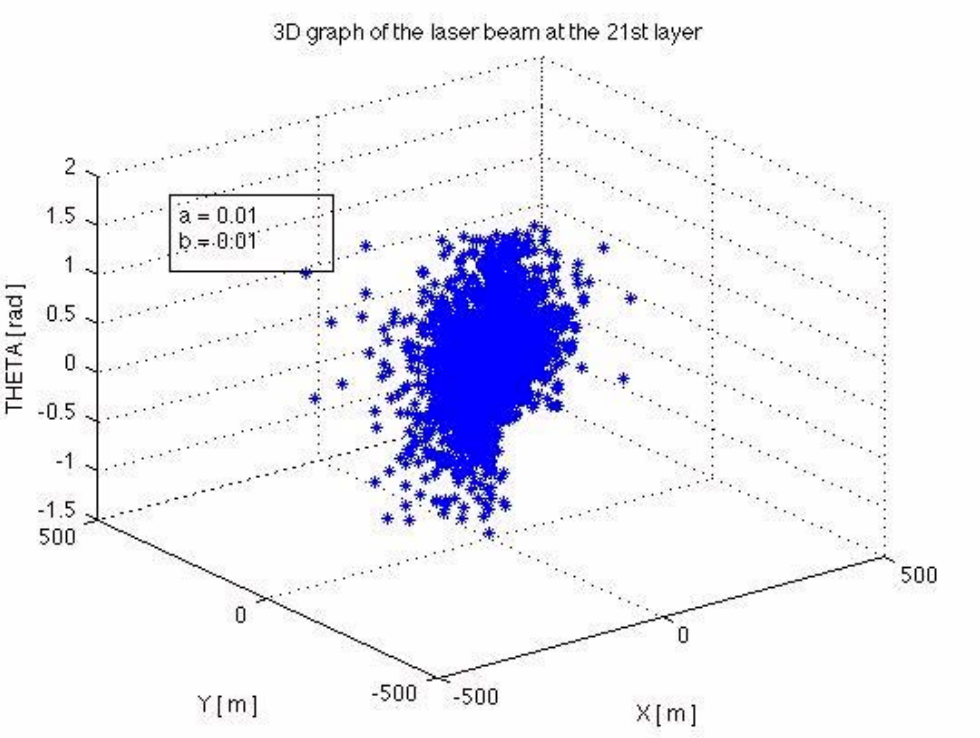

Figure 19. Light distribution at the twenty first layer for case I for 20 m

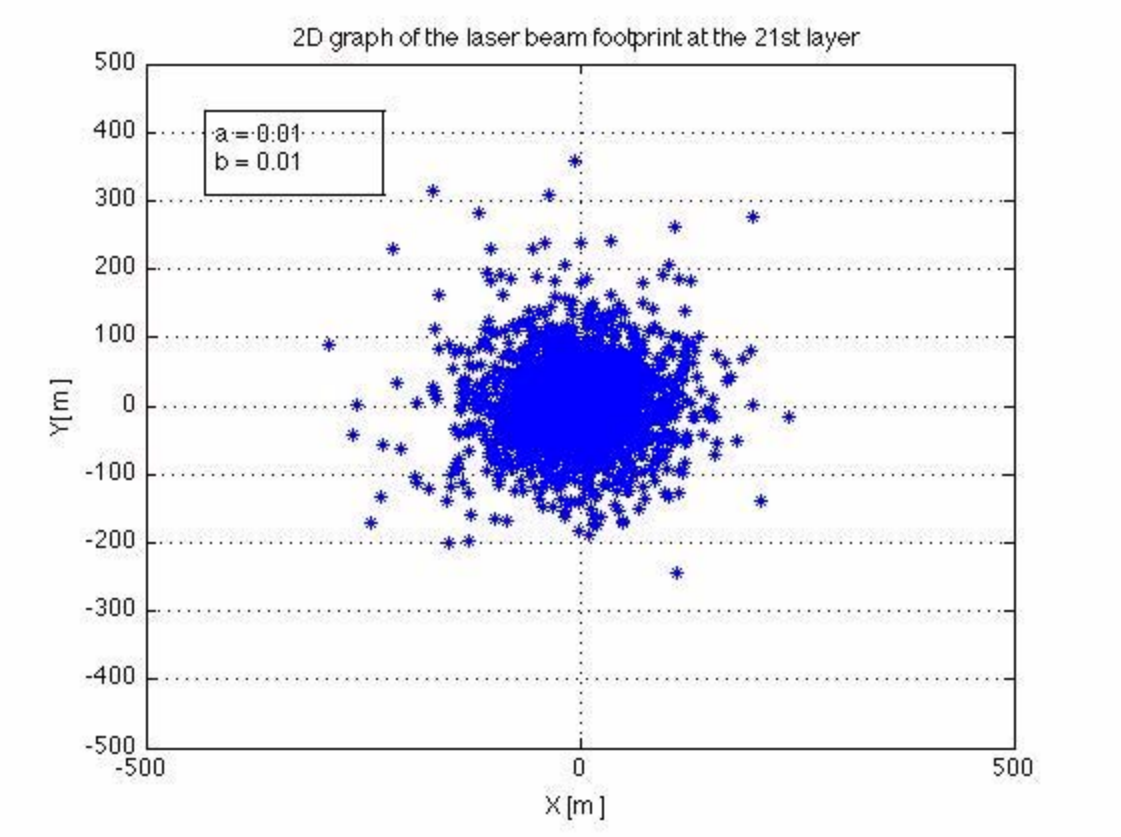

Figure 20. 2D Light distribution at the twenty first layers for case I for 20 m

2. Case II (Higher Extinction)

For this case, the following values will be assigned to the input parameters:

Absorption coefficient a = 0.5 1/m

Scattering coefficient b = 0.5 1/m

Depth interval = 0.5 m for a total depth of 10.5 m

Photon angle in the water = 90 degrees

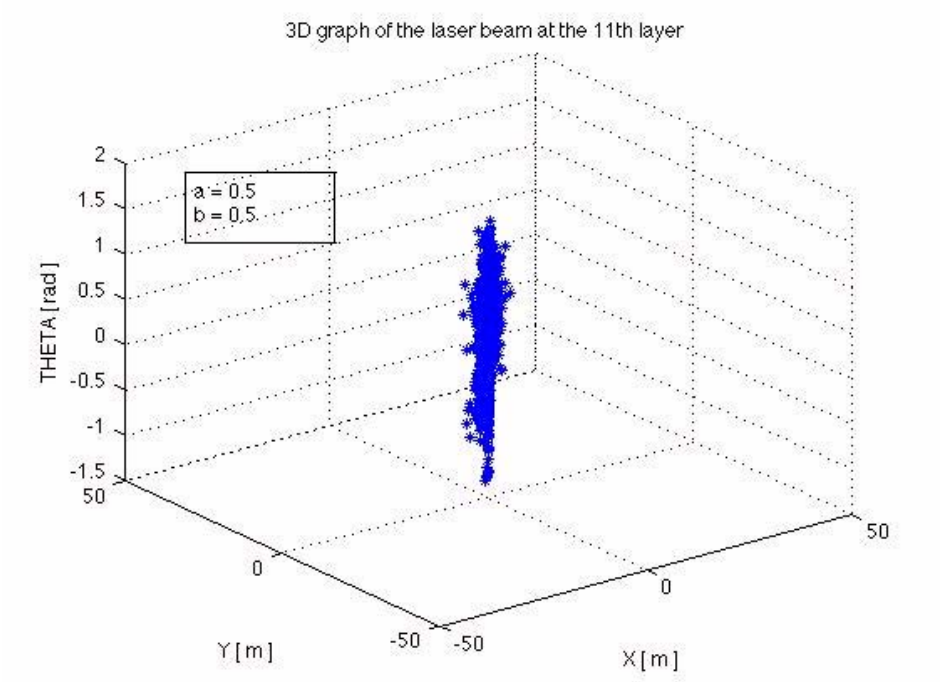

Figure 21. Light distribution at the eleventh layer for case II for 5 m

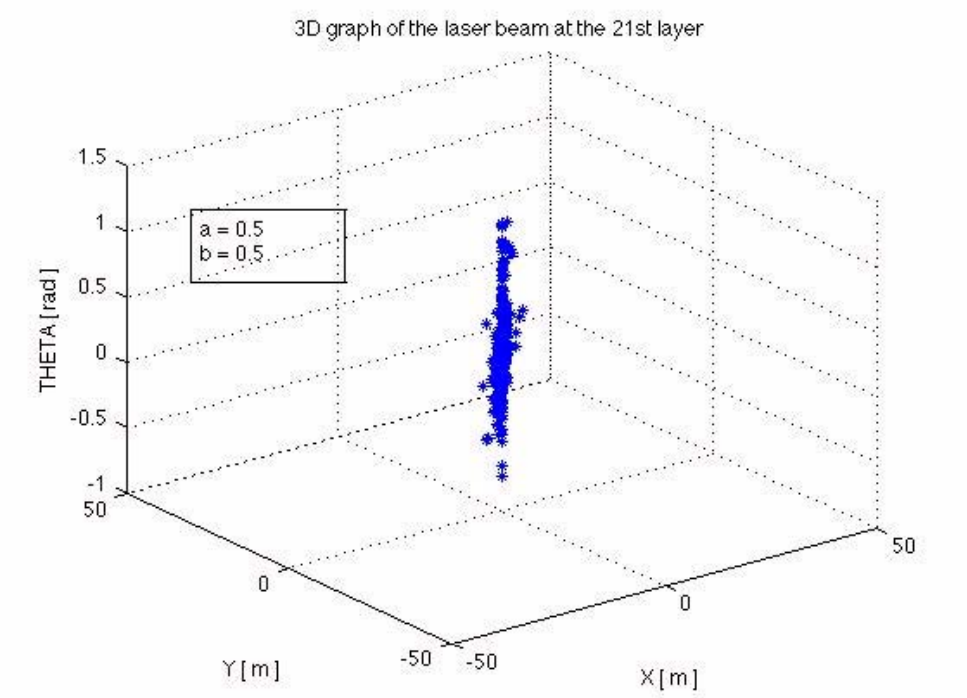

Figure 22. Light distribution at the twenty first layer for case II for 10 m

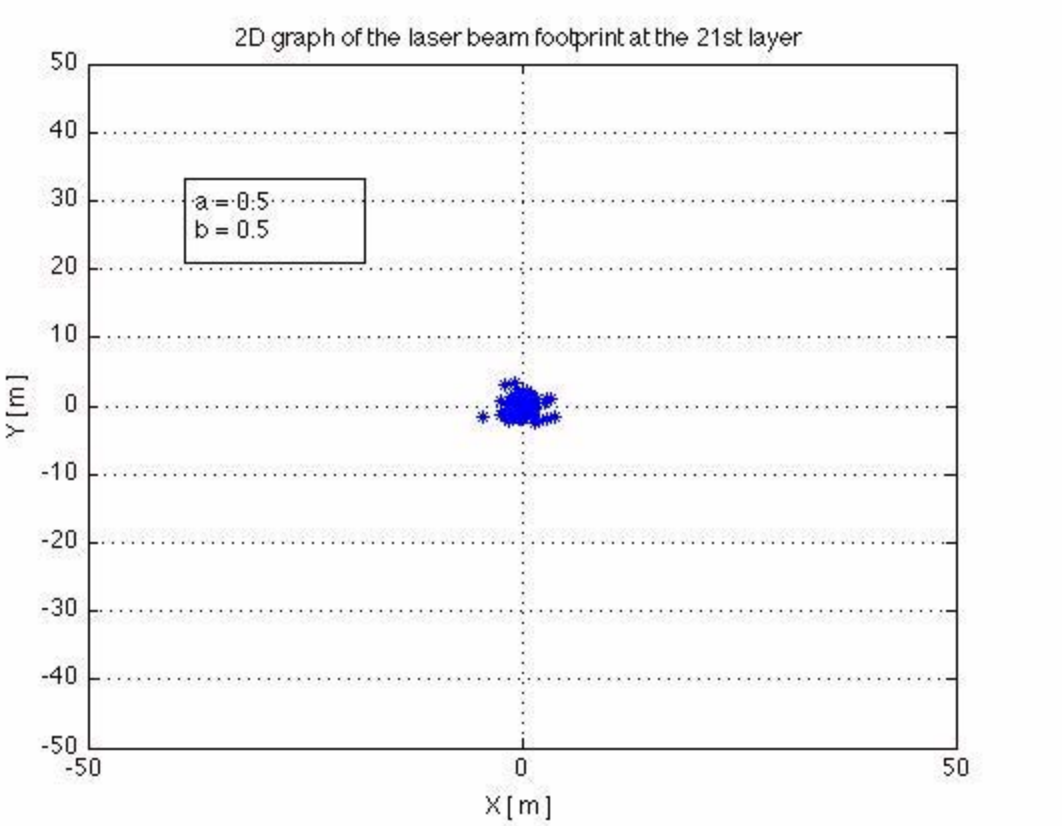

Figure 23. 2D Light distribution at the twenty first layer for case II for 10 m

3. Case III (Moderate Extinction)

For this case, the following values will be assigned to the input parameters:

Absorption coefficient a = 0.1 1/m

Scattering coefficient b = 0.1 1/m

Depth interval = 1 m for a total depth of 21 m

Photon angle in the water = 90 degrees

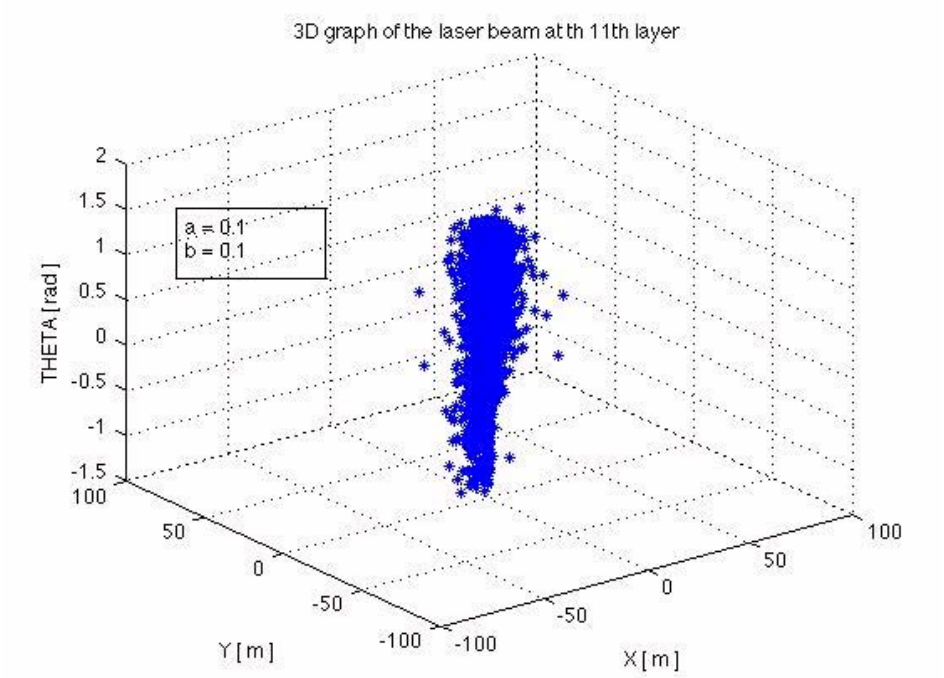

Figure 24. Light distribution at the eleventh layer for case III for 10 m

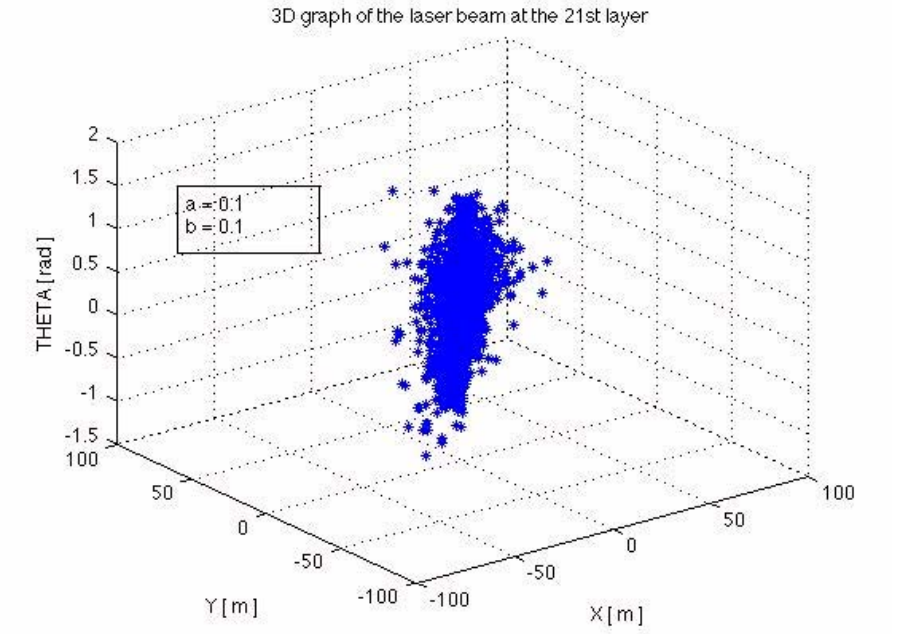

Figure 25. Light distribution at the twenty first layer for case III for 20 m

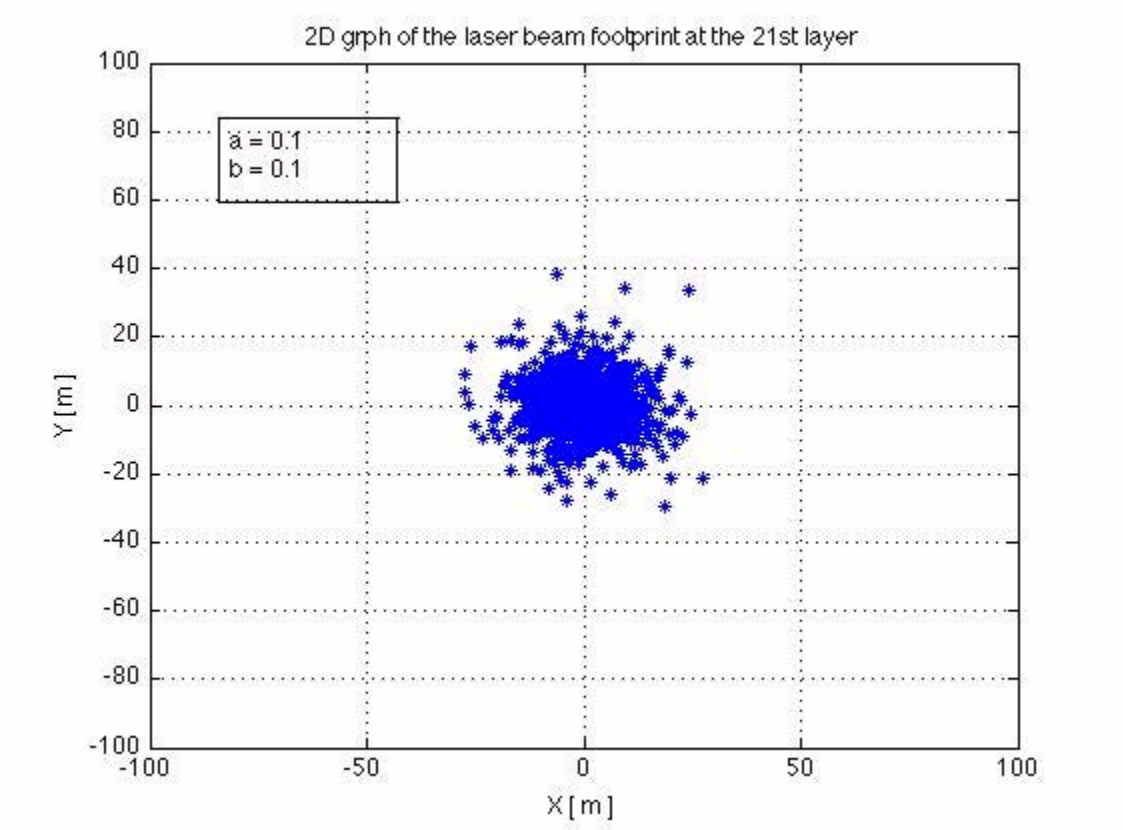

Figure 26. 2D Light distribution at the twenty first layer for case III for 20 m

C. INTERACTION WITH THE SEA SURFACE

This chapter evaluates the effect of the sea surface on the light distribution. Compared to Chapter III, the scattering and absorption influences of the water body before the interaction were included.

The light distribution just before the interaction was calculated in paragraph B of this chapter using both 3D and 2D graphs of the twenty-first layer for each case, as well as the corresponding data contained in the Kirk Code.

To demonstrate the spread of the laser beam as it exits the sea surface, a histogram of the exiting angle will be given for case III in comparison to the histogram of the scattering angle just before the interaction. For a wind speed of 10 m/sec the negligible difference between the two plots indicates the small effect of the ocean surface refraction.

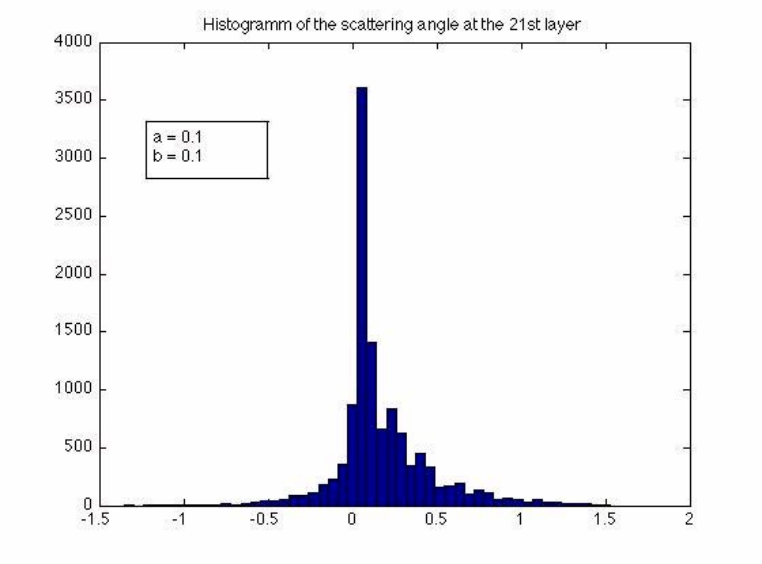

Figure 27. Scattering angle for absorption and scattering at the twenty first layer for case III. Standard deviation = 0.2842

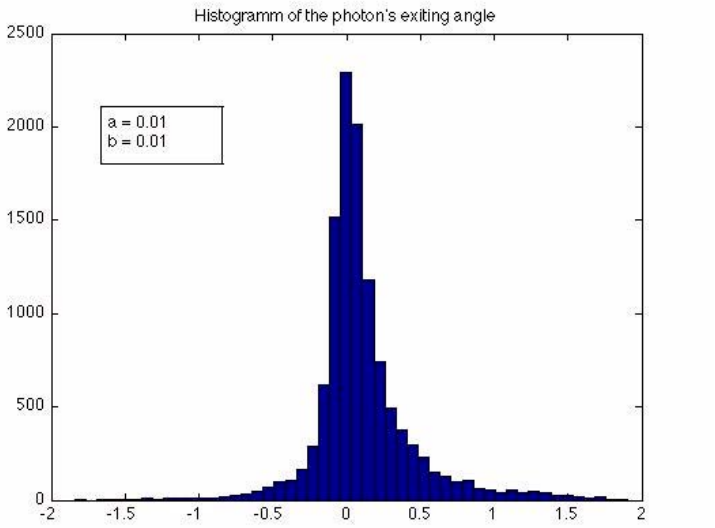

Figure 28. Angle spreading for absorption, scattering and refraction for case III .Standard Deviation = 0.3251

D. STANDARD DEVIATION

Applying the Kirk Code, a matrix table for standard deviation is next presented. It indicates the effect of scattering for the water depth of twenty one meters. As it can be

seen from Table 3, for constant absorption coefficient, standard deviation increases with increasing scattering coefficient, as expected. Finally, scattering appears to be more important after the value of 0.5 (1/m).

Table 3. Standard Deviation of the scattering angle for the depth of 21 m

a [1/m]\ b [1/m]	0.01	0.05	0.1	0.5
0.01	0.2826	0.2617	0.2434	0.2017
0.05	0.2947	0.2832	0.2548	0.2218
0.1	0.3317	0.3016	0.2852	0.2531
0.5	0.5044	0.4686	0.4443	0.3600

E. CHAPTER SUMMARY

This chapter, which is the core of the thesis, examines initially the spreading of the laser beam propagating inside a water body from scattering and absorption. It considers theoretical approach of the Monte Carlo and the Kirk Code and the simulation results. Examining the results, it can be seen that the dominant phenomenon is absorption compared to scattering. The upward light distribution was refracted at the sea surface, resulting in the beam pattern exiting the water. Comparing the histograms of the scattering and exiting angles it was found that the main effect is that of the scattering itself. Further, compared to scattering and absorption, the refraction at the surface does not substantially alter the beam pattern created as indicated by the corresponding standard deviations, which are very close.

VI. CONCLUSIONS AND RECOMMENDATIONS

A. THESIS CONCLUSIONS

A laser beam fired upward inside a water body experiences scattering and absorption that expands the beam of light. The absorption and scattering coefficients and the volume scattering function determine the angular spread. These parameters vary with wave length and the ocean water itself. The light distribution is then refracted at the ocean surface giving the final footprint of the beam, propagating in the air.

Among the two phenomena, known together as extinction, the absorption is the dominant one. Furthermore, no conclusions can be made based independently on absorption only or scattering only coefficients. This is because their action is simultaneous and combined. Generally the spread of the beam increases as absorption increases. The photons do not have the ability to propagate far, even for higher values of the scattering coefficient.

Between attenuation inside the ocean and scattering at the surface, the first is more important and mainly defines the shape and the size of the laser beam footprint.

B. RECOMMENDATIONS

Now that the laser beam footprint can be approximated, the attenuation due to propagation in the air and clouds should be considered. The objective is to obtain the final light distribution at the desired location.

Accordingly, when the laser beam is fired from the air into the water, the above results need to be considered.

Another issue, apart from the beam spreading, is the desired laser irradiance delivered on the target and the corresponding effectiveness.

THIS PAGE INTENTIONALLY LEFT BLANK

APPENDIX A

A. FUNDAMENTAL QUANTITIES

1. Radiant Flux {F}

The time rate of flow of radiant energy.

$\frac{W}{m^2}$, where Q is the radiant energy. Measured in W.

2. Radiance {L}

The radiant flux per unit solid angle per unit projected area of surface.

$L = \frac{d^2F}{dA \cdot \cos\varepsilon \cdot d\omega}$. asured in $\frac{W}{m^2 sr}$.

3. Irradiance {E}

Irradiance at a point of a surface is the radiant flux incident on an infinitesimal element of a surface containing the specific point, divided by the element area.

$E = \frac{dF}{dA}$. Measured in $\frac{W}{m^2}$.

THIS PAGE INTENTIONALLY LEFT BLANK

APPENDIX B: CODES

A. MATLAB CODE FOR GENERATING THE PIERSON-MOSKOWITZ NOISE FILTERED SPECTRUM AND CALCULATING THE MEAN-SQUARED SLOPE

```
% ocean surface and variance
%29 JULY 09

%constants
a = 0.0081;
b = 0.74;
g = 9.81; %gravity acceleration in m/sec^2
U = 10; %wind speed in m/sec
N = 2.^15; % number of points

% parameters
L = b.*g.^2./U.^4;
dk = 0.02; % linear stepsize of wavenumber
k = 1:N;
k = dk*k;
k2 = N/2;
k3 = k2+1;
k4 = 1:k2;
k5 = 1:k2-1;

% PM spectrum calculation

S = (a./(2.*k.^3)).*(exp(-(L./k.^2))); % PM spectrum in m^2/red/m
figure (1)
loglog(k,S)                              % PM spectrum graph
A = randn(1,N);                          %create an 1-D array of random
gaussian numbers
B = fft(A);                              % noise spectrum
C(1:N/2)=B(1:N/2).*sqrt(S(1:N/2));       % filter of noise spectrum with
PM spectrum
C(k3)=0;
C(k3+k5)=conj(C(k3-k5));
d = ifft(C);                             % inverse fft to distance
coordinates
dx = (2*pi)/(N*dk)                       %translate k into x distance
coordinates
x = dx*(1:N);
d = d*(sqrt(2*pi))/sqrt(2*dx);
figure (2)
plot(x,d)
xlabel('distance in m')
ylabel('height in m')

%variance calculation
```

```
variance= var(d)
Var     = dk.*sum(S)

%slope calculation
slope1 = dk*sum(k.^2.*S)
y      = diff((d)/dx);
slope2 = var(y)
slope3 = (a/4)* expint ((b*g^2)./(k(N).^2*U^4))
```

B. MATLAB CODE FOR GENERATING THE ELFOUHAILY NOISE FILTERED SPECTRUM AND CALCULATING THE MEAN-SQUARED SLOPE

```
% 06 August
%JONSWAP 1-D Spectrum

%  general costants
g  = 9.81;   %gravity acceleration      in m/sec^2
Cm = 0.23;   %capillary peak celerity   in m/sec
Km = 160;    %capillary peak wavenumber in 1/m
Xo = 22000;  % fetch constant
U  = 10;     % wind speed               in m/sec
N  = 2.^20;  % Number of points
X1 = 10^6;   % dimensional fetch        in m

% parameters
dk = 0.02;
k  = 1:N;    % wavenumber
k  = dk*k;
k2 = N/2;
k3 = k2+1;
k4 = 1:k2;
k5 = 1:k2-1;

% low frequency curvature spectrum Bl calculation
% special costants
Ko    = g/U.^2 ;
X     = (g*X1)/U^2;                              % non dimensional fetch
omega = 0.84 .*(tanh((X/Xo).^0.4)).^(-0.75);
Kp    = Ko.* omega.^2;                           % wavenumber of gravity
wave peak
Ap    = 0.006* sqrt(omega);                      % equilibrium range
parameter
Cp    = sqrt (g/Kp);                             % phase speed at
spectral peak
c     = sqrt (g./k);                             % phase speed
Lpm   = exp((-5/4).*((Kp./k).^2));               % PM spectral shape
s     = 0.08*(1+4.^ omega^-3);
GAMA  = exp(-((sqrt(k./Kp)-1).^2)/(2*s^2));
```

```
if omega <1
     gama = 1.7;
else gama = 1.7+ln(omega);
end

Jp    = gama.^GAMA;                              % JONSWAP peak
enhancement factor
Z     = exp( (- omega/sqrt(10)).*(sqrt(k./Kp)-1));
Bl    = (Ap/2)*(Cp./c).*Lpm.* Jp.*Z;             %low frequency
curvature spectrum
figure (1)
loglog(k,Bl)
xlabel('wavenumber k')
ylabel('low frequency curvature spectrum Bl')

%high frequency curvature spectrum Bh calculation

Zo    = 3.7*(10^-5)*(U^2/g)*(U/Cp)^0.9;          % roughness length
ustar = 0.42*U/log(10/Zo);                       %friction velocity

if ustar<Cm
Am = 0.01*(1+log(ustar/Cm));
else Am= 0.01*(1+3*log(ustar/Cm));
end

Bh = (Am/2)*(Cm./c).*exp(-0.25*((k./Km)-1).^2).*Lpm; %high frequency
curvature spectrum

figure (2)
loglog(k,Bh)
xlabel('wavenumber k')
ylabel('high frequency curvature spectrum Bh')
SPEC = (Bh+Bl)./k.^3;                            % 1-D  spectrum

% plotting the spectrum
figure(3)
loglog(k,SPEC)
xlabel('wavenumber k')
ylabel('elevation spectrum SPEC(k)')

% filtering the spectrum

A = randn(1,N);                          %create an 1-D array of random
gaussian numbers
B = fft(A);                              % noise spectrum
C(1:N/2)=B(1:N/2).*sqrt(SPEC(1:N/2));    % filter of noise spectrum with
PM spectrum
C(k3)=0;
C(k3+k5)=conj(C(k3-k5));
d  = ifft(C);                            % inverse fft to distance
coordinates
dx = (2*pi)/(N*dk);                      %translate k into x distance
coordinates
x  = dx*(1:N);
```

```
d  = d*(sqrt(2*pi))/sqrt(2*dx);

% plotting the noise filtered spectrum
Figure (4)
plot(x,d)
xlabel('distance in m')
ylabel('height in m')
title('noise filtered SPEC spectrum')

% variance calculation
variance = var(d)
VAR      = dk.*sum(SPEC)

% slope calculation
slope1 = dk*sum(k.^2.*SPEC)
y      = diff((d)/dx);
slope2 = var(y)
% slope3 = (a/4)* expint ((b*g^2)./(k(N).^2*U^4)) only for PM spec
```

C. MATLAB CODE FOR APPLYING SNELLS LAW TO ELFOUHAILY SPECTRUM MEAN-SQUARED SLOPE

```
% 09 sep 09
% apply snells law
%parameters
n1 = 1.3; % index of refraction for air
n2 = 1;   % index of refraction for water
scale = 0.01;

R    = y;                          % slope (R degrees from horizontal)
th1  =pi/4;                        % angle of incidence
th2  = asin((n1/n2)* sin(th1+R))-R; % angle of exiting
Vth2 = var(th2)
VR   = var(R)
Y    = Vth2/ VR
%D   = (1./sqrt(1-0.7^2 .*(sin(th1 + R)).^2)).*0.7.*cos(th1 + R) -1
%E   = D.^2
plot(th1,Y,'x')
hold on
title('ratio of variances vs th1 for wind speed 10')
gtext('N = 2^18, Km = 160')
```

LIST OF REFERENCES

[1] Nils Jerlov E.Steemann Nielsen, “Optical Aspects of Oceanography,” Academic Press, New York, NY, 1974.

[2] Shubha Sathyendranath, “Inherent Optical Properties of Natural Seawater,” National Institute of Oceanography, Donna Paula, 1984

[3] Nils Jerlov, “Marine Optics,” Amsterdam, 1976.

[4] Charles Cox and Walter Munk, “Statistics of the sea surface derived from sun glitter,” Scripps Institution of Oceanography, 1954.

[5] Willard J. Pierson and Lionel Moskowitz, “A proposed spectral form for fully developed wind seas based on the similarity theory by S. A Kitaigorodskii,’’ New York University, October 1963.

[6] Eric I. Thorsos, “Acousting scattering from a Pierson-Moskowitz sea surface,” University of Washington, WA, March 1954.

[7] Malcolm L. Heron, “Applying a unified directional wave spectrum to the remote sensing of wind wave directional spreading,” School of Mathematical and Physical Scienses, James Cook University, Townsville Australia, February 2002.

[8] T. Elfouhaily, B .Chapron and K. Katsaros, “ A unified directional spectrum for long and short wind-driven waves,” Journal of Geophysical Research, Vol 102, No C7, pp. 15781–15796, July 1997.

[9] Paul A. Hwang, “Wavenumber spectrum of intermediate-scale ocean surface waves,” Naval Research Laboratory, MS.

[10] Sherman Karp, Optical Channels, Fibers, Clouds, Water and the Atmosphere, San Diego, CA.

[11] Sherman Karp, “Optical Communications between Underwater and Above Surface (Satellite) Terminals,” San Diego, CA , July 1975.

[12] John T. O. Kirk, “ Monte Carlo Procedure for Simulating the Penetration of Light into Natural Water,” CSIRO Division of Plant Industry, Canberra, Australia, 1981.

[13] Raymond C. Smith and Karen S. Baker, “Optical classification of natural waters,” University of California, San Diego, La Jolla, 1978.

.

THIS PAGE INTENTIONALLY LEFT BLANK

INITIAL DISTRIBUTION LIST

1. Defense Technical Information Center
   Ft. Belvoir, Virginia

2. Dudley Knox Library
   Naval Postgraduate School
   Monterey, California

3. Chairman, Code PH
   Department of Physics
   Naval Postgraduate School
   Monterey, California

4. Professor Don Walters, Code PH/WA
   Department of Physics
   Naval Postgraduate School
   Monterey, California

5. Professor Brett Borden, Code PH/BO
   Department of Physics
   Naval Postgraduate School
   Monterey, California

6. Embassy of Greece
   Office of Naval Attaché
   Washington, District of Columbia

7. LTJG Xiradakis Pavlos
   Hellenic Navy General Staff
   Athens, Greece